View Article Online / Journal Homepage / Table of Contents for this issue
Dynamic Article Links

Journal of Materials Chemistry

Cite this: *J. Mater. Chem.*, 2011, **21**, 13705

www.rsc.org/materials

FEATURE ARTICLE

Recent progress in synergistic catalysis over heterometallic nanoparticles

Hai-Long Jiang and Qiang Xu*

Received 8th May 2011, Accepted 7th June 2011
DOI: 10.1039/c1jm12020d

Heterometallic nanoparticles (NPs) have been emerging as a type of important catalyst. Bimetallic NPs with alloyed and core–shell structures have higher activities than monometallic counterparts in catalysis due to the synergistic effects between the two metals. Compared to the straightforward synthesis of bimetallic alloy NPs, the preparation strategies for bimetallic core–shell NPs are flexible and diversified. In addition, synergistic catalysis over trimetallic and multimetallic NPs has also received considerable interest in recent years. In this feature article, we provide an overview of the recent developments of heterometallic NPs for improved catalytic performance.

Downloaded by University of Science and Technology of China on 06/05/2013 14:52:51.
Published on 08 August 2011 on http://pubs.rsc.org | doi:10.1039/C1JM12020D

1. Introduction

Metallic nanoparticles (NPs) or clusters, aggregates of several to millions atoms, have been emerging as a new type of important functional material.[1] They exhibit distinct properties (optical, electronic, magnetic, and so on) from those of individual atoms or their bulk counterparts due to the quantum-size and surface effects. More importantly, the properties are usually size- and structure-dependent, which have attracted tremendous research attention from either basic science or application viewpoints during the last two decades.[2–9]

Heterometallic NPs composed of two or more metal elements with various nanostructures (alloy/intermetallics, core–shell, heterostructure, *etc.*) *via* different synthesis approaches have presented improved physical and chemical properties compared to their monometallic NPs in many fields, especially in catalysis.[10,11] Since the properties of the catalyst surfaces are closely correlated with the catalytic activities, the precise modification of the catalyst surface by introducing another component or changing the morphology could facilitate the controlled tuning of the catalytic properties. In addition, for core–shell structured heterometallic NPs with the same shell composition, their catalytic activity can also be changed with the core metal due to the

National Institute of Advanced Industrial Science and Technology (AIST), Ikeda, Osaka, 563-8577, Japan. E-mail: q.xu@aist.go.jp; Fax: +81-72-751-9629; Tel: +81-72-751-9562

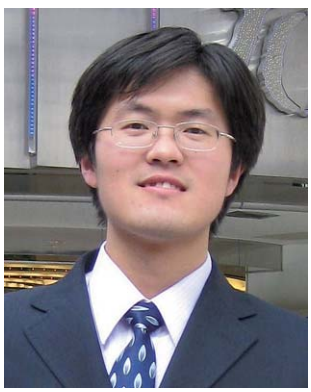

Hai-Long Jiang

Hai-Long Jiang was born in Anhui, P. R. China in 1981. He graduated from Anhui Normal University (2003) and obtained his PhD degree in inorganic chemistry from Fujian Institute of Research on the Structure of Matter, Chinese Academy of Sciences (CAS) in 2008 under the supervision of Prof. Jiang-Gao Mao. He then joined Prof. Qiang Xu's group at AIST as a postdoctoral fellow and became a JSPS (Japan Society for the Promotion of Science) fellow in 2009. He is currently interested in the development of porous materials and nanostructured materials for applications in catalysis, separation, sensing and hydrogen storage.

Qiang Xu

Qiang Xu received his PhD degree in physical chemistry in 1994 at Osaka University, Japan. After one year working as a postdoctoral fellow at Osaka University, he started his career as a Research Scientist at Osaka National Research Institute in 1995. Currently, he is a Senior Research Scientist at National Institute of Advanced Industrial Science and Technology (AIST, Japan), adjunct professor at Kobe University, and fellow of Royal Society of Chemistry (FRSC). His research interests include porous materials and nanostructured materials and related functional applications, especially for clean energy. He has published more than 200 papers in refereed journals.

Downloaded by University of Science and Technology of China on 06/05/2013 14:52:51.
Published on 08 August 2011 on http://pubs.rsc.org | doi:10.1039/C1JM12020D

so-called ligand effect. Therefore, the catalytic activity in catalysis can be well-tuned by combining two or more metals with various nanostructures. First principles studies have indicated the synergistic effect on the performance of heterometallic nanocatalysts is subject to surface electronic states, which are greatly altered by the change of catalysts for geometric parameters, particularly related to local strain and effective atomic coordination number at the surface.[12–14]

In recent years, great progress has been made and many examples have been reported in the preparation and synergistic catalysis of heterometallic NPs with the great efforts of researchers all over the world. In this feature article, we provide an overview of the recent developments of synergistic catalysis over experimental heterometallic NPs mostly based on the following three aspects: synergistic catalysis over bimetallic alloy NPs, preparation and synergistic catalytic effects of bimetallic core–shell NPs, as well as trimetallic and multimetallic NPs. Due to the large amount of reports on bi-/multi-metallic NPs and journal space limitations, we have only focused on experimental studies for the heterometallic NPs with catalytic synergy in the last 5–6 years. It should be noted here that some catalysts have not been defined to be alloyed or core–shell nanostructures, which we have also reviewed and marked with "undefined structure" due to the demonstrated synergistic catalysis between the metal species. In the last section, we will briefly discuss the current results progress, expected improvements and future outlook in this research area.

2. Synergistic catalysis over bimetallic alloy NPs

The chemical and physical properties of alloy NPs can be well tuned by varying the size, composition and atomic ordering. Generally speaking, alloy materials have distinct binding properties with reactants in contrast to those for monometallic metal catalysts. The strong metal–metal interactions tune the bonding between the catalyst surfaces and the reactants, where the extra stabilization of the transition state on the alloy catalysts in comparison to the corresponding interaction on the monometallic catalyst surface is an additional benefit. Usually, impregnation/co-reduction with a relatively strong reducing agent can be used for the preparation of bimetallic alloy NPs. The method is used in the synthesis of monometallic NPs but two metal precursors are co-introduced for bimetallic NPs. We classify and discuss the synergistic catalysis over plentiful nanoalloys according to their compositions as follows.

2.1 Alloy NPs involving two noble metals

Catalysis over Au–Pd alloy NPs has received the most attention among noble metal nanoalloys. Prati, Su and coworkers have systematically studied the selective oxidation catalysis over Au–Pd NPs obtained by a two-step procedure.[15–20] The bimetallic Au–M/C (M = Pd, Pt) catalyst (undefined Au–M structure) showed strong synergistic effect for liquid-phase oxidation of D-sorbitol in water using oxygen as oxidant, which produced not only a significant increase of reaction rate but also a system more resistant to oxygen poisoning allowing it to work under a moderate pressure.[15] In order to avoid the segregation of metal, the authors first immobilized a preformed Au sol (using BH_4^- as reductant) on activated carbon (AC), and then the Pd sol was generated in the presence of Au/AC using H_2 as the second reducing agent instead of $NaBH_4$ which usually led to Pd segregation. Slowing down the reduction rate of the Pd salt was regarded as the key to avoid Pd segregation or homogenous nucleation. Single phase bimetallic Au–Pd/AC showed high activity attributed to the synergistic effect between Au and Pd in the selective liquid-phase oxidation of glycerol towards glycerate using oxygen as the oxidant (Fig. 1). The strong synergistic effect was present in a large range of Au/Pd ratio, being maximized for the Au_{90}–Pd_{10} composition. In addition, the Au–Pd/AC catalyst exhibited a prolonged catalyst life although a small, inhomogeneous Pd leaching could be observed.[16–19] The Au–Pd alloys supported on AC with Au–Pd compositions ranging from 90 : 10 to 60 : 40 are also very active in the liquid-phase oxidation of alcohols such as benzylic alcohol, cinnamyl alcohol, octenol and octanol, confirming the high synergistic effect of the alloy. The addition of a base increases the activity of all catalysts with various Au/Pd ratios, and the extent of the enhancement is dependent on the nature of the alcohol to be oxidized and on the Au/Pd ratio.[20] Hutchings and coworkers have prepared Au–Pd alloy NPs with different methods which showed pronounced synergistic effects in redox catalysis.[21–23] By applying ZSM-5, zeolite β, zeolite Y, TS-1 and TiO_2 as supports for Au and Au–Pd NPs toward solvent-free oxidation of benzyl alcohol with oxygen, it was found that zeolite β was the best support for Au catalysts and the conversions were comparable to or better than those with TiO_2. However, the selectivities observed with the acidic zeolites were lower than those with the non-acidic TS-1 and TiO_2. The Au–Pd/zeolite-Y showed improved activity without significantly affecting the selectivity compared to the Au and Pd catalysts.[21] For the same reaction, the bimetallic Au–Pd NPs supported on CeO_2 was considerably more active than monometallic catalysts containing Au or Pd only. They adopted an antisolvent precipitation technique using supercritical CO_2 to prepare CeO_2 support for Au–Pd NPs, which was much more active than that prepared using a CeO_2 support derived from the acetate through a non-supercritical synthesis route.[22] The zeolite supported Au–Pd catalysts gave the highest activity for direct synthesis of hydrogen peroxide from H_2 and O_2 compared to supported Au, Au–Ru, Au–Rh and even Au–Pt catalysts prepared using a similar impregnation method.[23] Xing and coworkers have demonstrated that Au–Pd NPs have a unique characteristic to catalyze the decomposition of liquid formic acid for dramatically

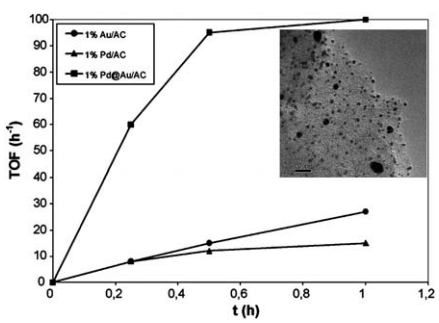

Fig. 1 Selective oxidation of glycerol with mono and bimetallic catalysts. Reaction conditions: water 10 ml, 0.3 M glycerol, glycerol/M = 3000, NaOH/glycerol = 4, $T = 50\ ^\circ C$, $P_{O_2} = 3$ atm. Inset: TEM image of fresh 1 wt% Pd–Au/AC catalyst. Scale bar: 20 nm. Adapted with permission from ref. 17. Copyright 2007, Elsevier.

 This journal is © The Royal Society of Chemistry 2011

Downloaded by University of Science and Technology of China on 06/05/2013 14:52:51.
Published on 08 August 2011 on http://pubs.rsc.org | doi:10.1039/C1JM12020D

and steadily evolving high-quality hydrogen at convenient temperature, the steady reaction activity of which is the highest among the investigated four catalysts (Pd/C, Pd–M/C, M = Cu, Ag, Au).[24] Recently, they have prepared an Au–Pd@Au core–shell nanostructure with Au–Pd alloy as the core supported on carbon. The catalyst possesses superior and stable activity as well as high selectivity at low temperature in hydrogen generation from formic acid decomposition. The reforming gas from formic acid decomposition contains only 30 ppm of CO and can be used directly in fuel cells. In contrast, there is a distinct deactivation effect after only 10 min for the Pd/C catalyst probably due to the formation of poisoning intermediates on the catalyst surface as the decomposition reaction goes on, although it is active for the decomposition reaction at the beginning. For Au/C catalyst, the catalytic activity is very low although the deactivation phenomenon was not observed.[25] Bimetallic PdAu alloy and core–shell NPs have been encapsulated into dendrimers, respectively by simultaneous and sequential metal loading/reduction. The catalytic hydrogenation of allyl alcohol was significantly enhanced in the presence of the alloy and core–shell PdAu NPs as compared to mixtures of monometallic NPs.[26] PVP-stabilized Au–Pd NPs (undefined Au–Pd structure) have been examined as catalysts for the oxidation of benzyl alcohol, 1-butanol, 2-butanol, 2-buten-1-ol and 1,4-butanediol in aqueous solution under mild conditions. It was found that Au–Pd NPs with Au/Pd ratio of 1 : 3 had higher catalytic activities than Au, Pd and other bimetallic Au–Pd NPs, and that the selectivities towards specific products can also be tuned using bimetallic NPs.[27] Silicon nanowires (Si NWs) were also used for supporting Au–Pd NPs (undefined Au–Pd structure) and the resultant Au–Pd/Si NWs exhibited the mutual promotional effect for the degradation of *p*-nitroaniline (*p*-NA) compared to Au/Si NWs and Pd/Si NWs. The synergistic effect factor was calculated as 2.35 and the Au–Pd/Si NW catalysts can be recycled and the catalytic rate only decreased by 20% after recycling for 4 times.[28] To maximize the interactions between the metallic precursor(s) and the activated carbon support in aqueous solution, Hermans *et al.* have studied the adsorption of Au and Pd species on activated carbon SX PLUS in order to prepare Au–Pd/C catalysts. The Au–Pd/C catalysts have been employed for the selective oxidation of glucose and exhibited higher activity than their monometallic counterparts, indicating a synergistic effect between the two metals.[29] A facile and fast microwave irradiation (MWI) method has been developed to prepare selected nanoalloys supported on ceria NPs for CO oxidation. The method allowed the passivation of the nanocrystals by using a mixture of oleylamine and oleic acid. High activity and thermal stability were observed for the nanoalloys according to the order CuPd > CuRh > AuPd > AuRh > PtRh > PdRh > AuPt.[30] The Pd NPs were immobilized on highly cross-linked polymer microspheres (PDVB-IL) without further surface modification of the polymer support. The loaded Pd NPs were nearly monodispersed and had high catalytic activity for cyclohexene hydrogenation reaction. Furthermore, the immobilized Pd NPs can be used as the seeds to prepare PDVB-IL-Pd/Au composites (undefined Au–Pd structure) by a seeding growth method. The Pd and Au in the composites have excellent synergy for catalyzing hydrogenation of cyclohexene.[31]

Mou, Zhang and colleagues have a series of reports on synergistic effect of bimetallic Au–Ag alloy nanocatalysts in CO oxidation.[32–36] The Au–Ag alloy NPs supported on mesoporous aluminosilicate, designated as Au–Ag@MCM, were prepared by one-pot synthesis using CTAB as both a stabilizing agent for NPs and a template for the formation of the mesoporous structure. The Au–Ag alloy NPs have larger particle sizes (>30 nm) whereas they exhibited much higher catalytic activity than Au NPs (~6.7 nm) in CO oxidation, which reveals that the size effect is not a critical factor whereas Ag is believed to play a key role in the activation of oxygen. The activity varies with the Au/Ag molar ratios and attains the best conversion when Au/Ag is 3 : 1. The reaction rate can reach 8.7×10^{-6} mol g_{cat}^{-1} s^{-1} at an Au/Ag molar ratio of 3/1 even at a low temperature of 250 K. The strong synergism in the co-adsorption of CO and O_2 on Au–Ag NPs was regarded as the crucial factor for the observed synergetic effect in catalysis.[32–34] Afterwards, they used silane APTS [$H_2N(CH_2)_3$–$Si(OMe)_3$] to functionalize the surface of mesoporous silica before adsorbing the gold precursor $AuCl_4^-$ and silver precursor $AgNO_3$ to afford Au–Ag bimetallic NPs inside the nanochannels after reduction. As compared with the previously reported Au–Ag@MCM prepared by a one-pot procedure, 4–6 nm bimetallic Au–Ag NPs were obtained *via* this two-step method. The small Au–Ag NPs exhibited higher activity in catalysis in the low-temperature CO oxidation with high stability and the catalyst was resistant to moisture over a long storage time. In addition, a synergetic effect in relative Au–Ag composition was also found.[35] In another report, they also adopted a two-step approach to prepare bimetallic Au–Ag NPs (Fig. 2). The Au NPs were first formed on amino-functionalized silica or alumina support, and then specific NPs were obtained with Au–Ag alloy core and Ag shell structure upon Ag^+ adsorption and reduction by $NaBH_4$. The obtained NPs were found to be highly thermally stable, and their sizes remain substantially unchanged (~3 nm) even upon calcination in air at 500 °C. After the final reduction with H_2, randomly distributed AuAg alloy NPs were obtained, which were very active toward CO catalytic oxidation, even superior to Au/TiO_2. The catalytic activities of $Au–Ag/SiO_2$ nanocomposites were dependent on Au/Ag ratio and much higher than Au/SiO_2 and Ag/SiO_2 catalysts.[36]

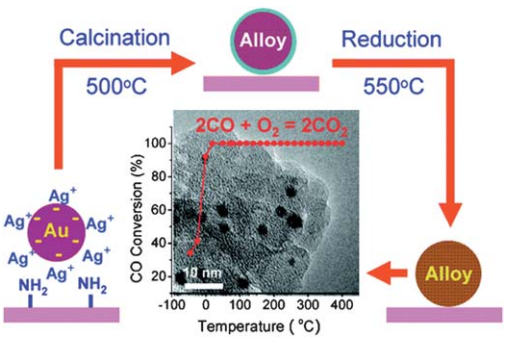

Fig. 2 Schematic illustration of preparation procedure for SiO_2 supported Au–Ag alloy NPs and HRTEM image as well as CO oxidation conversion of $Au–Ag/SiO_2$ (Au/Ag = 1/1). Gold NPs are formed on amino-functionalized silica, followed by Ag^+ adsorption. Upon reduction of Ag^+ by $NaBH_4$, NPs with a Au–Ag alloy core and a Ag shell are formed. These bimetallic NPs are highly stable up to 500 °C and further treatment *via* H_2 reduction results in a randomly distributed Au–Ag alloy, which is highly active for CO oxidation. Reproduced with permission from ref. 36. Copyright 2009, American Chemical Society.

Downloaded by University of Science and Technology of China on 06/05/2013 14:52:51.
Published on 08 August 2011 on http://pubs.rsc.org | doi:10.1039/C1JM12020D

Sun *et al.* have grown Ag nanoplates on GaAs substrates, where Ag was easily oxidized in ambient environments, resulting in the limitation of the potential applications of the nanoplates. They converted the Ag nanoplates on GaAs substrates into chemically stable nanoplates made of Au–Ag alloys. As a result, the alloy nanoplates retained the out-of-substrate orientation and highly exposed their surfaces to surrounding solutions, which were more resistant to oxidation and highly efficient for catalyzing the reduction of 4-nitrophenol with $NaBH_4$.[37] Wang *et al.* reported a one-pot synthesis of monodisperse AuAg alloy NPs with controlled compositions by simultaneous reduction of Au and Ag precursors in an organic solution with oleylamine as surfactant. The oleylamine was readily removed, leaving AuAg NPs that were catalytically active for CO oxidation. The composition-dependent catalytic activities revealed that the alloy NPs supported on fumed SiO_2 with Au/Ag ratio close to 1/1 had the highest activity in the CO oxidation.[38]

Currently, polymer electrolyte membrane (PEM) fuel cells are mostly based on expensive Pt-based electrocatalysts. Due to the limited supply of Pt and its susceptibility to poisoning by oxidation products, research endeavors have been focused on reducing or eliminating the Pt in fuel cell catalysts and increasing the resistance to poisoning. Lowering the quantity of Pt by alloying with another affordable metal (such as Au, Ru, Pd, *etc.*) is an alternative approach to solve this difficulty.[39–45] Tang *et al.* have investigated the electrocatalytic activity of electrochemically synthesized Au–Pt clusters deposited on fluorinated tin oxide (FTO) and carbon disk substrates in acidic and alkaline electrolytes. Both methanol oxidation reaction (MOR) and the oxygen reduction reaction (ORR) results showed that Pt could be partially substituted by Au to achieve higher resistance to poisoning without affecting the activity in acid electrolyte, while a significant overall improvement in performance was observed in alkaline environment, owing to a synergistic effect between Au and Pt.[40] The Au-modified Pt and Pt-modified Au electrodes were constructed and the surfaces were modified by the electrodeposition of sub-monolayers. Both types of Pt–Au surfaces were found to be more active for formic acid oxidation compared to bare Pt, showing the maximum activity at Pt fraction between 0.15 and 0.25 with the enhancement factor of more than two orders of magnitude.[41] Recently, Zhang *et al.* have prepared Au–Pt alloy NPs on graphene with uniform dispersion *via* a polyelectrolyte-assisted process. The resultant Au–Pt/graphene exhibited higher electrocatalytic activity and stability than Au–Pt/C and commercial Etek-Pt/C catalysts for formic acid oxidation.[43] The carbon supported Pt–Ru alloy NPs have been produced with poly (amidoamine) dendrimers (PAMAM) as a protective ligand in solution, which hinders particle sintering during activation at high temperature in H_2, and promotes the formation of highly disperse, bimetallic Pt–Ru NPs. It has been found that the catalyst with Pt/Ru ratio of 1 : 1 gave the best performance for MOR among Ru contents from 1 to 50 mol%.[44] The Pt_xPd_{1-x}/C nanocatalysts with various Pt/Pd atomic ratios ($x = 0.25, 0.5, 0.75$) have been synthesized by using a borohydride-reduction method. Rotating-disk electrode measurements revealed that the Pt_3Pd_1/C nanocatalyst had a synergistic effect on the ORR, showing 50% enhancement, and an antagonistic effect on the MOR, showing 90% reduction, compared to commercial JM 20 Pt/C on a mass basis. It was found that the ORR activity strongly depended on the Pt *d*-band vacancies and extent of alloying. A decrease in Pt *d*-band vacancy facilitates O–O scission, and thus enhances the ORR activity.[45] Nilekar *et al.* have deposited the Pt monolayers on different late-transition metals (Au, Pd, Ir, Rh, Ru), in which a Pd-supported Pt monolayer showed the highest ORR activity. Then they decreased the amount of Pt by replacing part of the Pt monolayer with a third late-transition metal (Au, Pd, Ir, Rh, Ru, Re, or Os). Several of these mixed Pt monolayers deposited on Pd single crystals or on carbon-supported Pd NPs exhibited up to a 20-fold increase in ORR activity on a Pt-mass basis compared to conventional all-Pt electrocatalysts. DFT calculations showed that their superior activity originated from the interaction between the Pt monolayer and the Pd substrate and from a reduced OH coverage on Pt sites, the result of enhanced destabilization of Pt–OH induced by the oxygenated third metal.[46]

Liu and coworkers have prepared bimetallic Au–Pt/TiO_2 for the efficient conversion of glycerol to lactic acid in high yields in alkaline aqueous solutions, which proceeds through glyceraldehyde and dihydroxyacetone intermediates formed from glycerol oxidative dehydrogenation as rate-determining step. Their results have demonstrated that the bimetallic Au–Pt/TiO_2 catalysts are stable and recyclable under the reaction conditions, which are in sharp contrast to the monometallic Au and Pt catalysts that showed dramatic decreases in their activities (Fig. 3).[47] Prati *et al.* have examined the catalytic activities of single-phase Au–Pd and Au–Pt on carbon supports for liquid-phase oxidation of glycerol and n-octanol. The synergistic catalytic effect between Au and Pt/Pd was proved to be considerable.[48] Bimetallic PtM (M = Au, Cu, Ni) alloy NPs supported on γ-Fe_2O_3 were synthesized by a radiolytic method by employing a 4.8 MeV electron beam to reduce aqueous ions without using any surfactant, organic solvent or stabilizer at room temperature. All the PtM/γ-Fe_2O_3 nanocomposites exhibited activities higher than those of Pt/γ-Fe_2O_3 catalysts in the CO oxidation. The correlation between the atomic structures and the catalytic activities indicated that the random alloy structure enhanced the activity.[49] Atomic layer deposition (ALD) was used to deposit Ru–Pt NPs with size of 1.2 nm supported on spherical alumina. Methanol decomposition reaction has confirmed the Ru–Pt interaction and showed improved methanol conversion over the bimetallic NPs compared to the catalyst comprised of a mixture of pure Pt and Ru NPs with

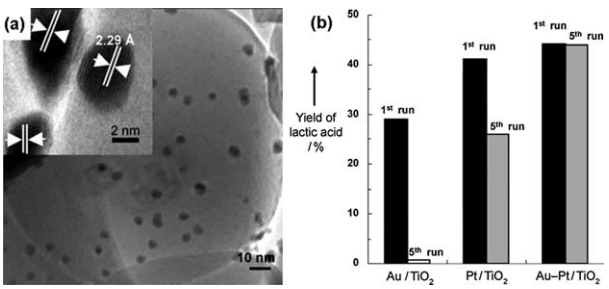

Fig. 3 (a) TEM image of Au–Pt/TiO_2 (Au/Pt = 1 : 1) before catalytic reaction. Inset: HRTEM image with marked lattice distance. (b) Yields of lactic acid after five reaction cycles at 363 K on Au/TiO_2, Pt/TiO_2, and Au–Pt/TiO_2 (Au/Pt = 1 : 1, 2.5×10^{-3} mmol metal, 0.22 mol L^{-1} glycerol in H_2O, NaOH/glycerol = 4 : 1 (mole ratio), 1 atm O_2). Adapted with permission from ref. 47. Copyright 2010, Wiley-VCH Verlag GmbH & Co. KGaA.

 This journal is © The Royal Society of Chemistry 2011

Downloaded by University of Science and Technology of China on 06/05/2013 14:52:51.
Published on 08 August 2011 on http://pubs.rsc.org | doi:10.1039/C1JM12020D

similar loading, revealing the synergistic catalysis between Pt and Ru in the alloy NPs.[50] Yoon *et al.* have studied carbon nanotube (CNT) supported metallic NPs for hydrogenation of neat benzene and its derivatives (toluene, 1-phenyl-1-cyclohexane) at room temperature without solvent, which cannot be achieved by commercially available carbon-based metal catalysts. The catalytic activity of the CNT-supported metallic NPs followed the order Pd–Rh > Pt > Rh > Au > Pd. The Pd–Rh bimetallic NP catalyst showed a strong positive synergistic effect compared to the individual single-component metal NP catalysts in the hydrogenation reaction.[51] Cao and Veser have synthesized Pt–Rh nanocatalysts with exceptional thermal stability *via* a microemulsion-mediated sol–gel process. The Pt–Rh NPs retained their diameter at 4 nm at calcination temperatures of up to 850 °C (Fig. 4a). This thermal stability of these NPs depends critically on the Pt/Rh ratio, having increased thermal stability with higher Rh content. The high thermal stability of Pt–Rh NPs has been considered to be responsible for their excellent catalytic performances over methane combustion. In contrast to the monometallic catalysts, the bimetallic PtRh–BHA (BHA: barium hexa-aluminate) sample not only showed enhanced activity with ignition of the CH_4/air stream at 450 °C and full CH_4 conversion around 550 °C (50–100 °C lower than those of the other samples, Fig. 4b); most importantly, it was stable over successive ignition–extinction cycles. Therefore, alloying Pt with Rh in the bimetallic PtRh–BHA catalyst allowed combination of the high activity of Pt with the thermal stability of Rh, resulting in a single nanostructured catalyst with exceptional stability and activity.[52] Likewise, Pt is prone to agglomeration at elevated temperatures, resulting in a decrease in the hydrogen yield, although it has long been regarded as an efficient catalyst for decomposition of hydrogen iodide (HI), one of the key reactions in the sulfur–iodine (S–I) thermochemical water splitting promising for massive hydrogen production. Studies have demonstrated that the synergistic effect of Pt and Ir with respect to HI decomposition was confirmed by the fact that the bimetallic Pt–Ir/C catalyst with 1 wt% and 0.77 wt%, respectively for Pt and Ir loadings showed much higher catalytic activity and thermostability compared with Pt/C and Ir/C catalysts.[53]

Hollow Ag–Pd alloy NPs were prepared by a galvanic displacement reaction, in which a small amount of $Pd(NO_3)_2$ was allowed to react with pre-synthesized Ag NPs as templates. The resultant hollow Ag–Pd NPs showed better catalytic activities than monometallic Ag and Pd NPs for electroless copper deposition (ECD) and the activities can be controlled by tuning their alloy ratios in a suitable manner.[54] It was reported that bimetallic

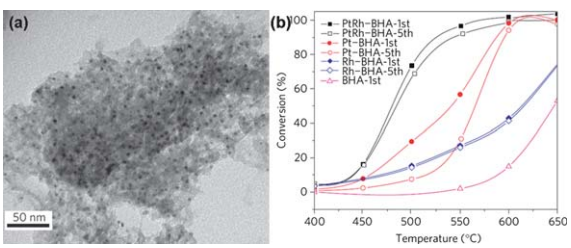

Fig. 4 (a) TEM image for PtRh–BHA calcined in air at 850 °C. (b) Methane conversion *vs.* reactor temperature in catalytic methane oxidation with three different BHA-based catalysts. Adapted with permission from ref. 52. Copyright 2010, Nature Publishing Group.

Ag–Rh/Al_2O_3 catalyst (undefined Ag–Rh structure) exhibited higher activity (for both nitrous oxide removal and hydrocarbon oxidation) than the monometallic counterparts for nitrous oxide (N_2O) reduction with methane and propene in the presence of oxygen (5%), due to the synergistic effect between Ag and Rh.[55] Afterwards, an ultrasound-assisted membrane reduction (UAMR) method was developed to construct highly dispersed Rh/γ-Al_2O_3 and bimetallic Au–Rh/γ-Al_2O_3 catalysts. The synergistic effect of the bimetallic system was found to improve the performance of selective catalytic reduction of NO and reduce the cost for Pt group metal-based catalysts. The Au–Rh/γ-Al_2O_3 (with alloy or core–shell structured Au–Rh NPs) catalyst with 0.33 wt% Au and 0.17 wt% Rh (M_{Rh}/M_{Au} = 1 : 1) loadings exhibited higher propylene and NO conversions than 0.5 wt% Rh/γ-Al_2O_3 catalyst and stronger NO adsorption capability and formation of surface nitrates have been confirmed over AuRh/γ-Al_2O_3 catalysts in NO-TPD experiments.[56]

2.2 Alloy NPs combining noble and non-noble metals

Many reports have indicated that alloying Pt with another non-noble metal can not only lower the cost but also effectively improve the catalytic properties of Pt NPs.[49,57–70] Bimetallic Pt–Ni NPs (undefined Pt–Ni structure) containing 0.5 wt% Pt and 20 wt% Ni have been prepared on activated carbon cloth (ACC) support for dehydrogenation of cyclohexane to benzene. The synergistic effect between Pt and Ni was obvious: the hydrogen production was enhanced by *ca.* 1.5 times as compared to the 20 wt% Ni-only catalyst and *ca.* 60 times higher hydrogen production rates as compared to 0.5 wt% Pt catalyst.[57] The Pt–Ni/HBEA (undefined Pt–Ni structure) catalyst prepared by ion exchange with simultaneous addition of Pt and Ni also showed the higher conversion and selectivity than Pt and Ni/HBEA in the reaction of n-hexane hydroisomerization, revealing the synergistic effect.[58] Silica supported Pt–Ni alloy NPs with a Pt/Ni ratio of 11/9 synthesized by the co-impregnation technique were more active than both pure monometallic catalysts in the catalytic hydrogenation of benzene. Surface segregation of Pt on the alloys as proven by XPS was regarded to contribute to this enhanced activity. However, Pt–Ni/SiO_2 prepared *via* a step-impregnated method showed lower catalytic reactivity than a pure Pt catalyst.[59] Our group has prepared Pt–Ni bimetallic nanocatalysts with a Pt content as low as 7 mol% by the co-reduction of the corresponding metal chlorides which exhibited excellent catalytic activity to the decomposition of hydrous hydrazine, producing hydrogen with a 100% selectivity at room temperature, whereas the corresponding single-component Ni and Pt counterparts were totally inactive for this reaction (Fig. 5).[60] Catalytic non-oxidative methane transformations into higher hydrocarbons over bimetallic Pt–Co NPs (undefined structure) supported on Al_2O_3 and NaY in a flow system have been investigated. The amount of C2+ products formed over the bimetallic catalyst were higher than that over the monometallic samples in the two-step process, with temperature ranging from 523 to 673 K and 1 bar pressure. The synergy in the bimetallic system can be explained by the enhanced reducibility of cobalt, increased metal surface (higher dispersion) and the cooperation of two types of active components (Co facilitates the chain-growth of partially dehydrogenated species produced on Pt in

Downloaded by University of Science and Technology of China on 06/05/2013 14:52:51.
Published on 08 August 2011 on http://pubs.rsc.org | doi:10.1039/C1JM12020D

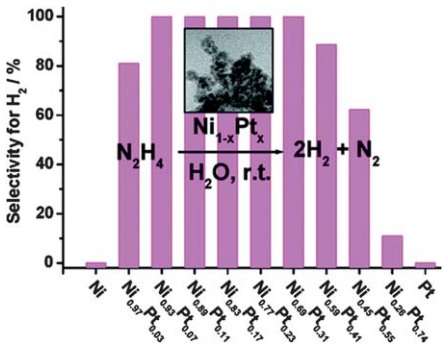

Fig. 5 Selectivities for hydrogen generation by the decomposition of hydrazine in aqueous solution (0.5 M) catalyzed by Ni, Pt, and $Ni_{1-x}Pt_x$ ($x = 0.03$–0.74) nanocatalysts at room temperature (catalyst = 0.017 g; $N_2H_4 \cdot H_2O$ = 0.1 mL). The inset TEM image showing $Ni_{0.93}Pt_{0.07}$ nanocatalyst after being used for the catalytic reaction. Reproduced with permission from ref. 60. Copyright 2010, American Chemical Society.

Pt–Co bimetallic NPs).[63] Ko *et al.* have reported that a Pt–Co bimetallic catalyst supported on yttria-stabilized zirconia (YSZ) was highly efficient for preferential CO oxidation (PROX) in a H_2-rich gas stream even with a small amount of Pt (0.5 wt%) at temperatures below 423 K. By optimizing the calcination and reduction pre-treatment conditions for Pt–Co/YSZ, the CO concentration can be decreased below 10 ppm in the temperature range of 380–423 K.[64] Highly dispersed Pt–Cu nanocrystals with 2 nm size were supported on $Mg_3Si_2O_5(OH)_4$ nanotubes or CeO_2, both of which showed enhanced performances compared to pure noble metal nanocrystals with similar sizes in the CO oxidation.[66] The combination of Pt and Sn metals, giving Pt–Sn bimetallic NPs supported on mesoporous carbon, have exhibited considerably higher conversion and selectivity in both the hydrogenation reaction of cinnamaldehyde to cinnamyl alcohol and the dehydrogenation reaction of propane to propylene, for the latter of which the presence of Sn resulting in higher Pt dispersion and weaker adsorption affinity of hydrocarbons on the surface Pt sites in Pt–Sn NPs may be responsible for the superior activity, selectivity and stability.[67,68] Nazar and coworkers have described a novel, highly effective methodology for impregnating noble metal Pt and bimetallic Pt–Bi NPs into ordered mesoporous carbon (OMC) voids with precisely controlled particle size (less than 3.5 nm in diameter) and ultra-high dispersion. The method is applicable to the preparation of other catalysts, such as Pt, Ru, Rh and Pd. The OMC-supported PtBi nanocrystallites between 2 and 3.5 nm were investigated as catalysts for formic acid electrooxidation. They displayed the same absence of CO poisoning as bulk intermetallic phases. The 3 nm Pt–Bi/OMC catalyst exhibited the highest mass activity for formic acid oxidation reported to date, under the same conditions, and over double that of Pt–Au. The excellent catalytic properties can be attributed to the successful catalyst preparation and the faithful occurrence of the "ensemble effect" at the nanoscale level.[70]

There are a couple of reports on synergistic catalytic effects over Au–Cu alloy NPs. Liu *et al.* have prepared Au–Cu alloy NPs with sizes of ~3 nm and a wide range of Au/Cu ratios on SBA-15 and silica gel supports and the catalysts on both supports with variational Au/Cu ratios showed superior CO oxidation activity to a monometallic Au catalyst, demonstrating the synergy between Au and Cu.[72,73] The Au–Cu NPs in the confined space of SBA-15 showed much better performance than monometallic NPs in catalyzing CO oxidation even with the rich presence of H_2. The Au–Cu/SiO_2 catalyst with an Au/Cu ratio of 20/1 gave the highest activity at room temperature while its activity showed the deepest valley with increasing reaction temperature; with an Au/Cu ratio of 3/1, it exhibited the best performance for PROX reaction. Hutchings and coworkers carefully reviewed the preparation methods, characterization techniques, theoretical studies and catalytic applications (in CO oxidation, propene epoxidation and benzyl alcohol oxidation) of Au–Cu alloy NPs in 2009.[74] Therefore, we will not give more details on Au–Cu nanocatalysts herein. Our group synthesized Au–Ni NPs (undefined structure) of 3–4 nm diameter embedded in SiO_2 nanospheres of around 15 nm prepared in a reversed-micelle system, and by *in situ* reduction in an aqueous solution of $NaBH_4/NH_3BH_3$. Compared with monometallic Au@SiO_2 and Ni@SiO_2, the as-synthesized Au–Ni@SiO_2 catalyst showed higher catalytic activity and better durability in the hydrolysis of NH_3BH_3, a promising reaction for chemical hydrogen storage and also an excellent test reaction for catalysis of nanomaterials,[75–77] generating a nearly stoichiometric amount of H_2 (Fig. 6). During the generation of H_2, the synergistic effect between Au and Ni was apparent: the Ni species stabilized the Au NPs and the existence of Au species improved the catalytic activity and durability of the Ni NPs.[78] Catalytic gas-phase hydrodechlorination (HDC) of 2,4-dichlorophenol (2,4-DCP) has been investigated over Ni/Al_2O_3 and Au/Al_2O_3 prepared by impregnation, and Au–Ni/Al_2O_3 (undefined Au–Ni structure) prepared by reductive deposition of Au onto Ni. The initial HDC performance converged for both Ni/Al_2O_3 and Au–Ni/Al_2O_3 but diverged with time on-stream as Ni/Al_2O_3 exhibited continual deactivation, while the combination of reaction with thermal treatment elevated the HDC performance of Au–Ni/Al_2O_3. The enhancement of HDC efficiency was assumed to be in correlation with the surface restructuring, which leads to Au–Ni clusters with a narrower (or more uniform) Ni–Au composition. A surface Ni–Au synergism was proposed whereby the Au

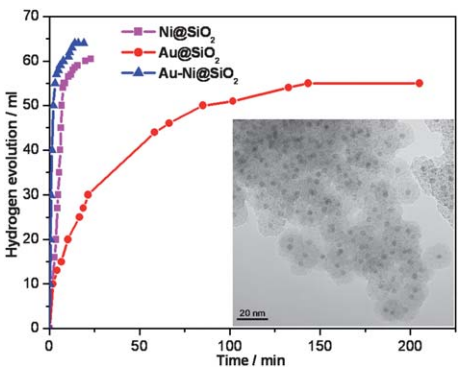

Fig. 6 Hydrogen generation by the hydrolysis of NH_3BH_3 (0.152 M, 5 mL) in the presence of the as-synthesized Ni@SiO_2, Au@SiO_2 and Au–Ni@SiO_2 catalysts (Au/AB = 0.019, Ni/AB = 0.065) at 18 °C in air (inset: TEM image of the as-synthesized Au–Ni@SiO_2 nanospheres). Reproduced from ref. 78 with permission. Copyright 2010, Wiley-VCH Verlag GmbH & Co. KGaA.

 This journal is © The Royal Society of Chemistry 2011

Downloaded by University of Science and Technology of China on 06/05/2013 14:52:51.
Published on 08 August 2011 on http://pubs.rsc.org | doi:10.1039/C1JM12020D

component served to activate the C–Cl bond(s) with subsequent attack from reactive hydrogen dissociated at the Ni centers.[79]

The γ-Al_2O_3 supported Ag–Cu NPs (undefined structure) were developed to catalyze glycerol to propanediols and showed a considerable synergistic effect, had superior activity and did not need a reduction pretreatment compared to the commercial copper chromite catalyst. It was revealed that the addition of Ag not only resulted in an *in situ* reduction of CuO, but also improved the dispersion of the Cu species on the support. The Ag–Cu/Al_2O_3 catalyst with optimal amounts of Cu and Ag showed a near 100% selectivity to propanediols with a glycerol conversion of about 27% under mild reaction conditions (200 °C, 1.5 MPa initial H_2 pressure, 10 h, (Cu + Ag)/glycerol molar ratio of 3/100).[80] A bimetallic Ag–Co/CeO_2 catalyst was prepared for simultaneous catalytic removal of NO and CO in the absence or presence of O_2. The addition of Ag on CeO_2 greatly improved the catalytic activities in the lower temperature regions (≤300 °C), and the introduction of Co on CeO_2 increased the activities at higher temperatures (≥250 °C). The bimetallic Ag–Co/CeO_2 catalyst combined the advantages of the corresponding individual metal supported catalysts and showed superior activity due to the synergetic effect. NO and CO could be completely removed in the range of 200–600 °C at a very high space velocity of 1.2×10^5 h^{-1}. No deactivation was observed over 4%Ag–0.4% Co/CeO_2 catalyst even after 50 h test.[81] The metastable alloyed Ag–Ni/SiO_2 catalysts (Ni + Ag = 1 wt%) were prepared by aqueous chemical reduction with hydrazine *via* precipitation or impregnation methods for gas-phase hydrogenation of benzene. The synergistic effect between Ni and Ag led to improvement of dispersion and reactivity of Ni in the presence of Ag for precipitated catalysts although Ag was inactive in the reaction.[82] Our group synthesized Rh_4Ni alloyed nanocatalysts with a particle size of ~3 nm by alloying Rh and Ni using a co-reduction process in the presence of hexadecyltrimethyl ammonium bromide (CTAB). A synergistic effect of Rh and Ni in the bimetallic Rh_4Ni nanocatalyst (Rh/Ni ratio = 4 : 1) was observed, over which a 100% selectivity for hydrogen generation by complete decomposition of hydrous hydrazine was achieved at room temperature.[83] Afterwards, a surfactant stabilized highly active bimetallic $Ni_{0.95}Ir_{0.05}$ alloy nanocatalyst was prepared by alloying Ir with Ni, which also exhibited 100% H_2 selectivity for complete decomposition of hydrous hydrazine at room temperature. Notably, the corresponding monometallic counterparts has poor H_2 selectivity (7% H_2 selectivity, Ir NPs; inactive, Ni NPs), highlighting the synergy in catalysis between Ir and Ni species.[84] In addition, supported bimetallic Ru–M (M = Ni, Co, Fe) and Pd–Co nanocatalysts have exhibited synergistic performances in the respective catalytic reactions.[85–88]

2.3 Alloy NPs involving two non-noble metals

Compared to bimetallic catalysts with noble metals, non-noble metal-based bimetallic NPs were much less studied, in which Cu–Ni catalysts have attracted the most interests.[89–93] Somorjai and coworkers have synthesized near-monodisperse $Ni_{1-x}Cu_x$ (x = 0.2–0.8) bimetallic nanocrystals by a one-pot thermolysis approach in oleylamine/1-octadecene, using metal acetylacetonates as precursors. The bimetallic nanocrystals deposited on silicon wafer displayed a catalytic synergistic effect in the hydrolysis of $NaBH_4$ to generate H_2 at $x = 0.5$ in a strongly basic medium. The $Ni_{0.5}Cu_{0.5}$ nanocrystals showed the lowest activation energy and exhibited the highest H_2 generation rate at 298 K.[89] Bimetallic Cu–Ni alloy NPs dispersed homogeneously on multi-walled carbon nanotubes (MWCNT), graphite oxide (GO) and activated carbon (AC) have been synthesized and all these catalysts displayed excellent catalytic activity for the direct synthesis of dimethyl carbonate (DMC) from CH_3OH and CO_2.[90–92] The Cu–Ni/MWCNT catalyst exhibited a conversion of CH_3OH higher than 4.3% and a selectivity of DMC higher than 85.0% under the optimal catalytic conditions of 120 °C and around 1.2 MPa. The high catalytic activity of Cu–Ni NPs could be attributed to the synergetic effects between Cu and Ni, Cu–Ni alloy in the activation of CH_3OH and CO_2, the unique structure of MWCNTs and the interaction between the metal NPs and the support. For Cu–Ni/GO catalyst, the highest CH_3OH conversion of 10.12% and the DMC selectivity of 90.2% were achieved under the optimal catalytic reaction conditions of 105 °C and 1.2 MPa. Christensen and coworkers have prepared a series of mono- and bi-metallic Fe–Ni catalysts supported on $MgAl_2O_4$ (spinel) and Al_2O_3 (alumina) and investigated their CO methanation activities. Bimetallic catalysts $Fe_{25}Ni_{75}$ and $Fe_{50}Ni_{50}$ showed significantly higher activities and in some cases also higher selectivities to methane in comparison with the traditional monometallic Ni and Fe catalysts. For the spinel support, the catalyst $Fe_{25}Ni_{75}$ was the most active at low metal loadings. With increasing metal concentrations, the maximum methanation activity was shifted to $Fe_{50}Ni_{50}$ on both spinel and alumina supports, and the maximum of the catalytic activity and the highest selectivity to methane were observed for the sample with 20 wt% total metal loading.[94] The $Fe_{1-x}Ni_x$ (x = 0, 0.3, 0.4, 0.5, 0.7 and 1) nano-alloys have been *in situ* synthesized and used as catalysts for H_2 generation from the aqueous NH_3BH_3 solution under ambient conditions. The prepared nano-alloys possess Pt-like high catalytic activity, especially for the specimen of $Fe_{0.5}Ni_{0.5}$, with which the hydrolysis of NH_3BH_3 could complete in only 2.2 min ($Fe_{0.5}Ni_{0.5}/NH_3BH_3$ = 0.12).[95] Some reported bimetallic alloyed nanocatalysts (involving some NPs with undefined structure) with synergistic effects in respective catalytic reactions are summarized in Table 1.

3. Synergistic catalysis over bimetallic core–shell NPs

Core–shell NPs are in the frontier of advanced materials chemistry among the various bimetallic NPs and are of great importance and interest owing to their physical and chemical properties that are strongly dependent on the structure of the core, shell, and interface, and also quite different from those of monometallic counterparts and alloys.[96] This structure dependence opens possibilities for tuning properties by controlling their chemical composition and the relative sizes of the core and shell.

3.1 Preparation strategy for bimetallic core–shell NPs

Compared to the general (one-step) straightforward synthesis of bimetallic alloy NPs, the preparation strategy for core–shell structured NPs is diversified and also a bit more complicated.

View Article Online

Downloaded by University of Science and Technology of China on 06/05/2013 14:52:51.
Published on 08 August 2011 on http://pubs.rsc.org | doi:10.1039/C1JM12020D

Table 1 Synergistic effects in catalysis over bimetallic alloyed NPs (some NPs with undefined structure are also included)

Catalyst	NP size (nm)	Catalytic reaction	Ref.
Au–M/AC (M = Pd, Pt)		oxidation of D-sorbitol	15
Au–Pd/AC	~3	oxidation of glycerol	16–19
Au–Pd/AC	~3	oxidation of alcohol	20
Au–Pd/zeolite-Y		solvent-free oxidation of benzyl alcohol	21
Au–Pd/CeO_2		solvent-free oxidation of benzyl alcohol	22
Au–Pd/zeolite		direct synthesis of H_2O_2 from H_2 and O_2	23
Au–Pd/AC	~4	H_2 generation from formic acid	24
Au–Pd@Au/C	~16	H_2 generation from formic acid	25
Au–Pd@dendrimer	~2	hydrogenation of allyl alcohol	26
Au–Pd	2.5–4.0	oxidation of alcohol	27
Au–Pd/Si NWs	15	degradation of *p*-nitroaniline	28
Au–Pd/C		oxidation of glucose	29
AuM (M = Pd, Rh, Pt), RhM (M = Cu, Pt, Pd)		CO oxidation	30
Au–Pd/polymer microspheres	8–9	hydrogenation of cyclohexane	31
Au–Ag@MCM	20–50	CO oxidation	32–34
Au–Ag@APTS-MCM	4–6	CO oxidation	35
Au–Ag/SiO_2	~3	CO oxidation	36
Au–Ag/GaAs substrate		reduction of 4-nitrophenol	37
Au–Ag/SiO_2	8–9	CO oxidation	38
Au–Pt/C	~3	methanol electrooxidation	39
Au–Pt clusters on FTO substrates/carbon disks		MeOH electrooxidation, oxygen reduction	40
Au modified Pt or Pt modified Au electrodes		formic acid oxidation	41
Au–Pt	2	methanol electrooxidation	42
Au–Pt/graphene	3.3 ± 0.2	formic acid oxidation	43
G4OH–Pt–Ru	3–5	methanol electrooxidation	44
Pt–Pd/C	4–6	MeOH electrooxidation, oxygen reduction	45
Pt or PtM modified Pd (M = Au, Ir, Rh, Ru, Re)		oxygen reduction reaction	46
Au–Pt/TiO_2	2.7–3.8	aerobic oxidation of glycerol	47
Au–M/C (M = Pd, Pt)	2.5–3.5	oxidation of glycerol and n-octanol	48
PtM/γ-Fe_2O_3 (M = Au, Cu, Ni)	2–3	CO oxidation	49
Ru–Pt/Al_2O_3	1.2	methanol decomposition	50
Pd–Rh/CNT	4.6 ± 1.0	hydrogenation of benzene	51
PtRh–BHA	~4	catalytic methane combustion	52
Pt–Ir/C	5.4	decomposition of hydrogen iodide	53
hollow Ag–Pd		electroless copper deposition	54
Ag–Rh/Al_2O_3		nitrous oxide reduction with CH_4 and propene	55
Au–Rh/γ-Al_2O_3	3–7	reduction of NO by propylene	56
Pt–Ni/ACC	~9	dehydrogenation of cyclohexane to benzene	57
Pt–Ni/HBEA		n-hexane hydroisomeriszation	58
Pt–Ni/SiO_2	2.5 ± 0.7	hydrogenation of benzene	59
Pt–Ni	~5	decomposition of $N_2H_4 \cdot H_2O$ to H_2	60
Pt–Ni/γ-Al_2O_3	~1.6	reduction of NO with H_2	61
Pt–Ni/CB		CO oxidation	62
Pt–Co/NaY		methane conversion to higher hydrocarbons	63
Pt–Co/YSZ	2.9 ± 0.5	PROX in H_2-rich gas stream	64
Pt–Co/CNT	1–5	hydrogenation of cinnamaldehyde to cinnamyl alcohol	65
Pt–Cu/silicate nanotube or CeO_2	~2	CO oxidation	66
Pt–Sn/CX-18		hydrogenation of cinnamaldehyde to cinnamyl alcohol	67
Pt–Sn/SBA-15	10	dehydrogenation of propane to propylene	68
Pt–Bi/C	~40	oxygen reduction reaction	69
Pt–Bi/OMC	<3.5	HCOOH and MeOH electrooxidation	70
Pt–Mo/γ-Al_2O_3		hydrodesulphurization (HDS) reaction	71
Au–Cu/SBA-15	~3	CO oxidation	72
Au–Cu/SiO_2	3.0–3.6	CO oxidation	73
Au–Ni@SiO_2	3–4	dehydrogenation of aqueous NH_3BH_3	78
Au–Ni/Al_2O_3	1–30	hydrodechlorination of 2,4-dichlorophenol	79
Ag–Cu/γ-Al_2O_3		hydrogenolysis of glycerol to propandediols	80
Ag–Co/CeO_2		conversion of NO and CO to N_2 and CO_2	81
Ag–Ni/SiO_2	8–30	gas-phase hydrogenation of benzene	82
Rh–Ni	~3	decomposition of $N_2H_4 \cdot H_2O$ to H_2	83
Ir–Ni	~5	decomposition of $N_2H_4 \cdot H_2O$ to H_2	84
Ru–Ni/SiO_2		hydrodechlorination of 1,2-dichloroethane	85
Ru–Fe/$MgAl_2O_4$	1–10	water-gas shift reaction	86
M–Co/SiO_2 (M = Rh, Ru)		oxidative steam reforming of ethanol to H_2	87
Ru–M/SiO_2 (M = Co, Fe)		NO-promoted N_2O decomposition	88
Ni–Cu/Si wafer	~20	hydrolysis of $NaBH_4$ to generate H_2	89
Cu–Ni/MWCNT	5–30	direct synthesis of dimethyl carbonate	90
Cu–Ni/MWCNT	~25	direct synthesis of dimethyl carbonate	91

 This journal is © The Royal Society of Chemistry 2011

Table 1 (*Contd.*)

Catalyst	NP size (nm)	Catalytic reaction	Ref.
$Cu–Ni/SiO_2$	~25	acetylene hydrogenation	93
$Fe–Ni/MgAl_2O_4$ and Al_2O_3	8–12	CO methanation	94
Fe–Ni	~3	dehydrogenation of aqueous NH_3BH_3	95

Downloaded by University of Science and Technology of China on 06/05/2013 14:52:51.
Published on 08 August 2011 on http://pubs.rsc.org | doi:10.1039/C1JM12020D

Herein, we would like to introduce several mostly accepted approaches for the fabrication of bimetallic core–shell NPs.

The successive two-step reduction for core and shell NPs, respectively, is almost universal to prepare core–shell bimetallic NPs. The deposition of the shell metal on the pre-formed core metal NPs seems to be very effective. To this end, however, a second metal must be deposited on the surface of the pre-formed particles, and the pre-formed metal NPs should be chemically surrounded by the deposited element. Xia and coworkers have prepared Pd@Au core–shell nanocrystals with controlled Au shell thickness *via* an epitaxial growth approach. They firstly synthesized Pd nanocubes with an average edge length of 10 nm in an aqueous solution by reducing Na_2PdCl_4 with L-ascorbic acid in the presence of bromide ions as capping agents. With the obtained Pd nanocubes as seeds, they overgrew Pd@Au nanocrystals by reducing $HAuCl_4$ with L-ascorbic acid in aqueous solution. The Pd cores retained their original cubic shape during the deposition of Au shells. TEM observation showed that the Au overlayers completely covered the main faces of the Pd nanocubes and also the continuous lattice fringes from the Pd core to the Au shell, indicating an epitaxial relationship between the two metals.[97] Tsuji *et al.* have prepared Au@Cu and Au@Ag core–shell nanocrystals using a two-step reduction method.[98,99] The Au core seeds with different shapes were prepared by reducing $HAuCl_4$ in ethylene glycol (EG) or tetraethylene glycol (TEG) under microwave heating in the presence of PVP as a polymer surfactant. Then the Cu or Ag shells were overgrown on the Au core seeds under oil-bath heating conditions. Although a large mismatch exists in lattice constants between Au (0.4079 nm) and Cu (0.3615 nm), the flat {111} facet of Cu shells were grown epitaxially on {111} facets of Au cores. Sánchez-Iglesias *et al.* have fabricated Au@Ag core–shell nanostructures with controlled morphology at room temperature through epitaxial growth of Ag onto the surface of single-crystal Au nanorods, using hydroquinone as reduction agent for selective reduction of Ag^+ ions. The presence of methoxy-poly (ethylene glycol)-thiol preferentially bound at the Au nanorod tips seems to completely block Ag growth in the longitudinal direction, thereby inducing a notable reshaping of the particles, with a subsequent decrease of aspect ratio, and ultimately leading to single-crystal octahedra, which get rounded through lamellar twinning upon further reduction. The morphology and thus the optical properties of these core–shell nanostructures can be finely tuned by controlling the amount of Ag grown on the particle surface.[100] In the successive two-step reduction approach, it is fairly difficult to obtain the core–shell NPs on the sub-10 nm scale, especially in the absence of a stabilizer/surfactant. With the limitation effect of the pore/surface structure of a metal–organic framework (ZIF-8), a new type of porous functional material,[101] we have successfully fabricated Au@Ag NPs within 2–6 nm without the help of a surfactant by a sequential deposition–reduction route for Au and Ag. The deposition in a reverse order for Au and Ag also produced similar core–shell nanostructures while the shell was composed of AuAg alloy, caused by the galvanic replacement reaction due to the differences in reduction potentials of the two soluble metal salts ($E^\circ_{Ag^+/Ag} = +0.80$ eV *vs.* SHE; $E^\circ_{Au^{3+}/Au} = +0.93$ eV *vs.* SHE) (Scheme 1).[102] The stepwise synthesis was also employed for successful preparation of triple-layered Pd@Au@FePt NPs, in which Pd@Au NPs served as NP seeds for further FePt shell coating.[103]

Although the two-step reduction/epitaxial growth method is general but a bit complicated, a one-step route for bimetallic core–shell NPs has also been developed recently, in most of which a suitable reducing agent for the metal cations with differential reduction potentials is very important. Our group reported a rational strategy for fabricating magnetically recyclable Au@Co core–shell NPs through the one-step seeding-growth route at room temperature under ambient atmosphere within a few minutes. The one-step synthetic method was achieved by exposing a mixture of Au^{3+} and Co^{2+} precursors to the reducing agent NH_3BH_3 simultaneously, where Co^{2+} cannot be reduced while Au NPs can be formed first by reduction of Au^{3+} with NH_3BH_3 and then act as a catalyst for hydrolytic dehydrogenation of NH_3BH_3 to afford active –H species. The pre-formed Au NPs served as the *in situ* seeds and the produced

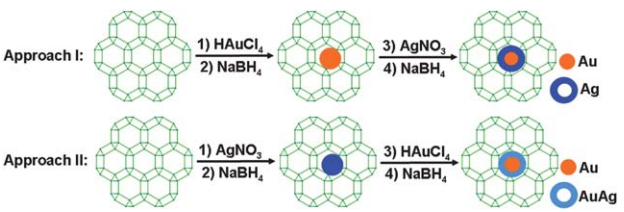

Scheme 1 Schematic illustration for the preparation routes of Au@Ag and Au@AuAg core–shell NPs. Reproduced with permission from ref. 102. Copyright 2011, American Chemical Society.

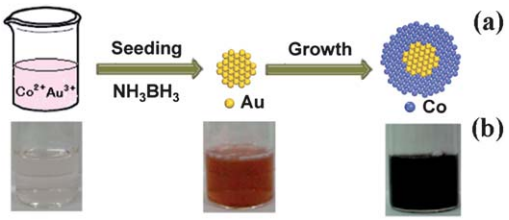

Scheme 2 (a) Schematic illustration, (b) color evolution in the formation process of Au@Co core–shell NPs *via* a one-step seeding-growth method at room temperature. Reproduced with permission from ref. 104. Copyright 2010, American Chemical Society.

Downloaded by University of Science and Technology of China on 06/05/2013 14:52:51.
Published on 08 August 2011 on http://pubs.rsc.org | doi:10.1039/C1JM12020D

active –H species reduced Co^{2+} for the successive growth of outer Co shells (Scheme 2). Therefore, the basic concept of this one-step synthesis of the Au@Co core–shell NPs is to take advantage of the different reduction potentials of the two metal salts ($E^{\circ}_{Co^{2+}/Co} = -0.28$ eV *vs.* SHE; $E^{\circ}_{Au^{3+}/Au+} = 0.93$ eV *vs.* SHE), where NH_3BH_3 as a moderate reducing agent is essential. It is worthy to note here that use of a strong reducing agent (for example, $NaBH_4$) will result in the formation of alloy NPs whereas use of a very weak reducing agent (for example, alcohol) cannot yield NPs or give only Au NPs because Co^{2+} cannot be reduced.[104] Following a similar strategy, non-noble metal-based bimetallic core–shell NPs have also been prepared by using NH_3BH_3 as reducing agent, demonstrating the generality of this method.[105] Wang and Li have also presented a one-pot wet chemical route to the synthesis of Au@Co core–shell nanocrystals and Au–Ni spindly nanostructures, in which a suitable reducing agent, octadecylamine (ODA), is crucial for their success. In the ODA solvent, M^{2+} (M = Co, Ni) cannot be reduced whereas Au^{3+} and M^{2+} can be co-reduced based on the following reduction mechanism: the Au^{3+} can obtain electrons from ODA and be reduced to Au (step I). Once the Au forms, it is surrounded by an electron cloud offered by free electrons of other Au atoms. M^{2+} cannot be directly reduced by either ODA or Au, but it can be adsorbed on the surface of Au and share a small portion of the electron cloud through its empty orbital (step II). This causes the spherical electron cloud distribution surrounding Au to become an elliptical distribution. The shift in the electron cloud leads to a partial positive charge on the Au surface, which is immediately neutralized by electrons offered by ODA. The continual supply of electrons from ODA to Au makes the shift in the electron cloud from Au to M occur continuously until M^{2+} is reduced completely.[106] Most recently, Huang *et al.* have used bayberry tannin (BT), a natural plant polyphenol, as a reducing agent for the one-step synthesis of Au@Pd core–shell NPs in aqueous solution at room temperature. Due to its mild and stepwise reduction ability, BT was able to preferentially reduce Au^{3+} to Au NPs when placed in contact with an Au^{3+}/Pd^{2+} mixture, and subsequently, the formed Au NPs served as *in situ* seeds for the growth of a Pd shell, resulting in the formation of Au@Pd NPs. Importantly, it is feasible to adjust the morphology of the Pd shell by varying the Pd^{2+}/Au^{3+} molar ratio, where Au@Pd NPs with a spherical Pd shell are formed when the Pd^{2+} amount is insufficient, whereas NPs with a cubic Pd shell are formed when Pd^{2+} is sufficient.[107] Han and coworkers have also reported one-step aqueous synthesis of bimetallic Au@Pd core–shell NPs with a well-defined octahedral shape, in which cetyltrimethylammonium chloride (CTAC) as both reductant and stabilizer is very critical and cannot be substituted by ascorbic acid or CTAB.[108] Similarly, triple-layered Au@Pd@Pt core–shell NPs have been synthesized by using ascorbic acid as a special reducing agent,[109] which we will discuss in detail in Section 4.

Carpenter and coworkers have also reported one-pot aqueous synthesis of Fe@Ag or Ag@Fe core–shell NPs, in which they have shown that the injection time of $AgNO_3$ into a reaction vessel containing aqueous ferrous salt, sodium borohydride, and sodium citrate is a vital parameter for the precise control of a desired core–shell structure. Scheme 3 depicts how the introduction of $AgNO_3$ at different times after the addition of $NaBH_4$ creates various core/shell structures. The results can be explained

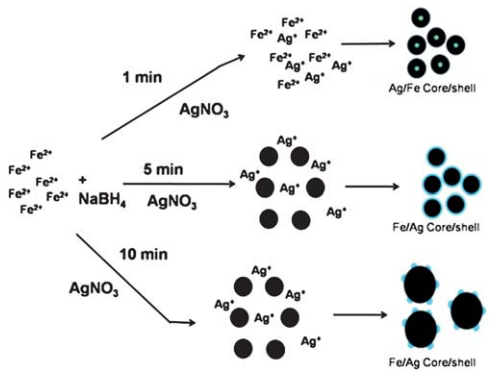

Scheme 3 Proposed reaction scheme for the reduction of sodium citrate, $FeCl_2 \cdot 7H_2O$ and $NaBH_4$; addition of $AgNO_3$ at various times after the addition of $NaBH_4$ produced various core–shell morphologies. Reproduced with permission from ref. 110. Copyright 2010, American Chemical Society.

by the differences in the reduction potentials for Fe^{2+} and Ag^{+} in an aqueous solution ($E^{\circ}_{Fe^{2+}/Fe} = -0.41$ V *vs.* SHE; $E^{\circ}_{Ag^{+}/Ag} = +0.80$ V *vs.* SHE). For the introduction in 1 min after $NaBH_4$ addition, Ag is formed by classical homogeneous nucleation and growth, resulting in 4–5 nm spherical NPs. These Ag NPs serve as nucleation sites for the Fe NPs to grow, which simulates a heterogeneous nucleation and growth process. For the introduction after 5 min, the Fe NPs have already formed and therefore act as nucleation sites for the Ag NPs to form and grow, creating Fe@Ag core–shell NPs. Lastly, the introduction after 10 min produces ~150 nm Fe clusters and these Fe clusters again act as nucleation sites for the formation of Ag shells.[110]

Galvanic replacement is an effective approach to fabricate bimetallic core–shell NPs with hollow interiors based on the differences in the reduction potentials of core and shell metal ions. Xia and coworkers have devoted much in this topic and developed a lot of bimetallic core–shell NPs.[111] The shell metal is mostly noble metals whereas core metal could be either noble or non-noble metals.[111–113] In addition, it is also very effective for fabricating yolk–shell/nanorattle structured NPs[113–115] or core–shell NPs with alloy shells.[102,116]

It is known that alloy NPs can usually be obtained from bimetallic core–shell NPs by high-temperature annealing or even by a process of hydrogen absorption/desorption as a trigger for Pd@Pt NPs reported recently.[117,118] There are also some interesting transformations from alloy to core–shell NPs (Scheme 4). Mayrhofer *et al.* have found that PtCo@Pt core–shell NPs can be obtained from Pt_3Co alloy upon CO annealing at 200 °C, where the adsorption enthalpy of CO on Pt is higher than on Co, Pt segregates to the surface of the NPs, and correspondingly displaces Co to the core.[119] Subsequently, carbon supported

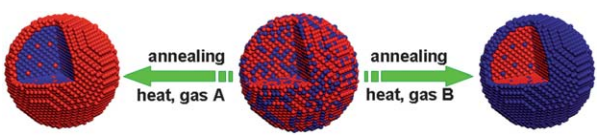

Scheme 4 Structural transformation from alloy to bimetallic core–shell NPs *via* reaction-driven processes.

 This journal is © The Royal Society of Chemistry 2011

Downloaded by University of Science and Technology of China on 06/05/2013 14:52:51.
Published on 08 August 2011 on http://pubs.rsc.org | doi:10.1039/C1JM12020D

PdCo@Pd core–shell NPs have been prepared *via* annealing PdCo/C at 500 °C under flowing H_2 based on the segregation effect induced by the difference in the gas adsorption energies on the two metals. Under the high temperature annealing conditions, the PdCo/C alloys undergo phase segregation in which Pd migrates to the surface, forming a pure Pd overlayer on the bulk alloy to afford PdCo@Pd NPs, since the adsorption enthalpy of H on Pd is higher than that on Co.[120] More interestingly, Tao *et al.* have studied that the $Rh_{0.5}Pd_{0.5}$ NPs undergo dramatic and reversible changes in composition and chemical state in response to oxidizing or reducing conditions. The NP with Rh rich in the surface can be detected upon exposure to an oxidizing gas of NO, while Rh atoms can move back to the core if the NP is exposed to a reducing gas of CO. Thus, the use of reactive gases is a rather unique way to engineer the structures of bimetallic core–shell-like NPs.[121]

Toshima and coworkers have proposed three possible routes for preparation of heterometallic core–shell NPs based on their long-term and systematic studies: 1) Pt@Pd core–shell NPs have been obtained by simultaneous gentle reduction with alcohol for H_2PtCl_6 and $PdCl_3$ in the presence of PVP; 2) Pd@Pt core–shell NPs have been prepared by a so-called hydrogen-sacrificial protective strategy, in which hydrogen adsorbed on the surface of core-metal NPs works as reductant of the second metal ions to produce the shell; 3) physical mixture of two kinds of metal NP in dispersions can spontaneously produce core–shell-structured bimetallic NPs. They have even succeeded in construction of a triple core–shell structure by combination of sacrificial hydrogen reduction or simultaneous alcohol reduction with a physical mixing process (self-organization).[122] Kim *et al.* have reported the formation of CNT supported core–shell clusters in the shape of nano-dandelions on the atomic scale in which the core is a single Pt atom and the shells are several agglomerated Ru atoms. Such an interesting structure resulted from the difference of bond strengths with sulfur atoms in thiol groups between Pt and Ru single atoms which formed onto surface thiol groups of CNT by borohydride reduction; the Ru–S bond is much weaker than the Pt–S bond. This brings about the faster release of Ru atoms from thiol groups than from Pt atoms during heat treatment; then, the drifting Ru atoms cover the Pt single atoms still linked to surface thiol groups and form a nano-dandelion structure (Scheme 5). The main advantage of this unique synthetic strategy for core–shell clusters compared to the conventional method is that it is possible to synthesize very small core–shell clusters below 1 nm in size.[123] In addition, Zhang *et al.* reported a well-controlled synthetic strategy to achieve meticulous control of metallic shell growth at the single monolayer level with versatile core NPs *via* introducing an intermediate phase in a phase transfer reaction to finely tune the shell growth process.[124] Yang *et al.* have reported a general protocol for transferring metal ions from water to an organic medium by using ethanol as an intermediate solvent. The protocol enables the synthesis of a variety of metallic nanocrystals, including core–shell NPs, to be carried out in an organic medium using relatively inexpensive water-soluble metal salts as starting materials.[125]

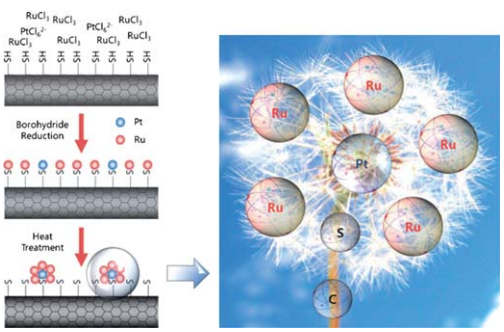

Scheme 5 PtRu nano-dandelion formation mechanism based on a single atom to cluster approach. Reproduced with permission from ref. 123. Copyright 2010, The Royal Society of Chemistry.

3.2 Core–shell NPs involving two noble metals

Similar to alloy NPs, core–shell structured bimetallic Au–Ag and Au–Pd NPs are preferentially studied among core–shell NPs because of their wide uses in different ends, especially their efficient catalytic properties for a variety of reactions. The electrocatalytic activity of core–shell $Au_{100-x}@Ag_x$ ($x = 15, 27, 46, 60$) bimetallic NPs embedded in a methyl functionalized silicate MTMOS network towards the reduction of hydrogen peroxide was investigated by using cyclic voltammetry and chronoamperometric techniques. The MTMOS silicate sol–gel embedded $Au_{73}@Ag_{27}$ core–shell NP modified electrode showed a synergistic effect and better electrocatalytic activity compared to monometal MTMOS–Au_{nps} and MTMOS–Ag_{nps} modified electrodes.[126] Toshima and coworkers have interests in Ag@Au core–shell catalysts for glucose oxidation. The addition of $AgClO_4$ into aqueous dispersions of Au NPs was applied to produce bimetallic Ag@Au NPs with a core–shell structure. The catalytic activity for glucose oxidation was investigated for thus-prepared Ag@Au

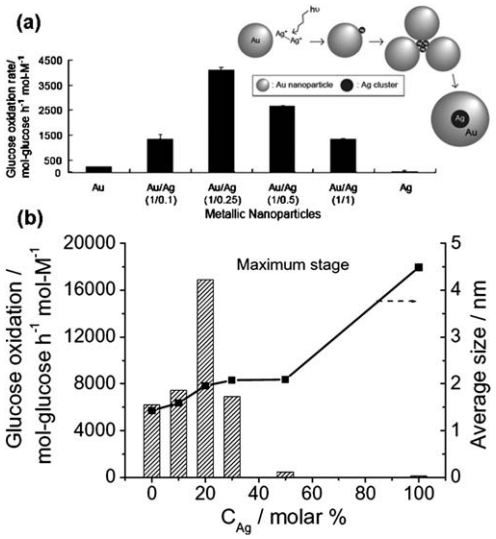

Fig. 7 (a) Glucose oxidation catalytic activity of Ag@Au NPs at various feed composition ratios and Au and Ag monometallic NPs. Inset: schematic presentation of the formation of Ag/Au bimetallic NPs by the addition of $AgClO_4$ aqueous solution into Au NP dispersion. (b) Catalytic activity on glucose oxidation and particles size of Ag@Au bimetallic NPs prepared at various feeding compositions (final metal ion concentration = 0.20 mM, $R_{PVP} = 100$, $R_{NaBH4} = 5$). Adapted with permissions from ref. 127 and 128. Copyrights 2010, American Chemical Society and 2011, Elsevier, respectively.

Downloaded by University of Science and Technology of China on 06/05/2013 14:52:51.
Published on 08 August 2011 on http://pubs.rsc.org | doi:10.1039/C1JM12020D

bimetallic NPs with various compositions. The highest activity (4079 mol-glucose h^{-1} mol-M^{-1}) was observed for the Ag@Au NP prepared with an Ag/Au ratio of 0.25/1, much higher than that of monometallic Au or Ag NPs under the same conditions. The high catalytic activity of the Ag@Au NPs may be due to the electronic effect between the Au and Ag elements in a particle (Fig. 7a).[127] More recently, they have developed a simple and novel one-pot preparation method for PVP-protected Ag@Au bimetallic NPs of less than 2 nm in diameter using simultaneous reduction of the corresponding ions with rapid injection of $NaBH_4$. The Ag@Au bimetallic NPs showed a high and durable catalytic activity for the aerobic glucose oxidation, and the catalyst can be stably kept for more than 2 months under ambient conditions. The highest activity was observed for the bimetallic NPs with Ag/Au atomic ratio of 2/8, of which the TOF value (16 890 mol-glucose h^{-1} mol-metal^{-1}) was several times higher than that of Au NPs with nearly the same particle size and much higher than that of Ag NPs (Fig. 7b).[128]

Tang *et al.* have synthesized spherical Ag–C composites with Ag NPs by microwaving suspensions of porous carbon spheres (CSs) in $[Ag(NH_3)_2]^+$ solutions with poly(*N*-vinylpyrrolidone) as the reducing agent. The obtained Ag–C composites were used as precursors to dope Au into the CSs' interior by immersing Ag–C composites in $HAuCl_4$ solution without additional reducing agent, thus yielding bimetallic Au–Ag/C composites with possible hollow Ag@Au core–shell structure due to the galvanic replacement reaction. Optical properties and catalytic activities of the composite were tunable *via* simply controlling the Au/Ag atomic ratio as controlled by the $HAuCl_4$ concentration. The catalytic activity of bimetallic composites was highly enhanced than that of the monometallically doped CSs in the reduction of 4-nitrophenol by $NaBH_4$.[129] Our group have fabricated Au@Ag or Au@AuAg NPs confined with an ZIF-8 support for catalytic reduction of 4-nitrophenol. Results showed the highly synergistic improvement for the catalytic activity compared to the monometallic and alloy NPs. The apparent activation energy for the most active catalyst, 2wt%Au@2wt%Ag/ZIF-8, was evaluated to be 14 kJ mol^{-1}, which was much lower than those reported for Au- or Ag-based catalysts and further illuminated the synergistic effect of Au and Ag species.[102]

Crooks and coworkers have prepared dendrimer-encapsulated PdAu bimetallic NPs in 1–3 nm with alloyed and core–shell Pd–Au structures, respectively by simultaneously and sequentially loading metal precursors into the dendrimer and following by reduction. The catalytic hydrogenation of allyl alcohol was significantly enhanced in the presence of core–shell structured Pd–Au NPs as compared to mixtures of single-metal NPs.[130] The Pd-on-Au bimetallic NPs with a 4 nm Au core and controlled Pd loading were synthesized, with all compositions more active for the aqueous-phase trichloroethene hydrodechlorination (TCE HDC) reaction. The most active catalysts were considerably more active (>1900 L g_{Pd}^{-1} min^{-1}) than Pd NPs (55 L g_{Pd}^{-1} min^{-1}) and conventionally synthesized Pd/Al_2O_3 (47 L g_{Pd}^{-1} min^{-1}). The reaction data suggested geometric effects were responsible for enhanced TCE HDC activity. The binding energy shifts of Pd metal with surface coverage suggested the possibility of catalyst promotion by an electronic effect.[131] Hutchings and colleagues have found that the addition of Pd to the Au catalyst, yielding Al_2O_3 supported bimetallic Au@Pd core–shell NPs with a Pd-rich surface, increased the rate of direct hydrogen peroxide synthesis from H_2 and O_2 as well as the concentration of hydrogen peroxide formed.[132] Almost simultaneously, they reported the Au@Pd NPs with Au-rich core and Pd-rich shell supported on TiO_2 gave very high TOFs (up to 270 000 turnovers per hour) for the oxidation of alcohols, including primary alkyl alcohols. The catalytic results showed that the introduction of Au to Pd improved the selectivity to aldehydes and Au acted as an electronic promoter for Pd to influence the catalytic properties.[133] Frank *et al.* have also demonstrated that Au@Pd NPs can be effectively supported by aqueous titania dispersion in absence of any organic stabilizing ligands with excellent colloidal stability. Without the need for drying and sintering, $Au_{70}@Pd_{30}/TiO_2$ was catalytically active in aqueous oxidation of 1-phenylethanol by hydrogen peroxide with good conversions at 75 °C and appreciable activity at 25 °C, which was much higher than the activity of pure Pd/TiO_2 and Au/TiO_2.[134]

Zhang *et al.* have fabricated a novel Pt-around-Au nanocomposite (similar to core–shell structured Au@Pt) by electrostatic self-assembly. It exhibited significantly enhanced activity and high stability towards formic acid oxidation, which showed a promising application in direct formic acid fuel cells. The proposed reason for the unexpectedly high activity for HCOOH oxidation on the Pt-around-Au nanocomposite was the efficient spillover of HCOO from Au to the surrounding Pt NPs, where HCOO is further oxidized to CO_2.[135] Ataee-Esfahani *et al.* have synthesized Au@Pt nanocolloids with nanostructured dendritic Pt shells by one-step chemically reducing H_2PtCl_6 and $HAuCl_4$ species with ascorbic acid in the presence of a low-concentration surfactant solution under simple ultrasonic irradiation conditions. The Pt shell thicknesses on Au cores can be readily tuned by controlling the Pt/Au molar ratio in the starting precursor solution. Through the optimization of the Pt shell thickness, the Au@Pt nanocolloids exhibited enhanced activity as an electrocatalyst for methanol oxidation reaction, which was ~4 times as high as that of the dendritic Pt nanocolloids while Au nanocolloids were almost inactive.[136] Han and coworkers have prepared bimetallic heteronanostructures consisting of a dendritic Pt shell and structured Au cores (nanocubes, nanorods, and nanooctahedra) *via* a seeded growth method. The Au@Pt nanostructures have exhibited higher electrocatalytic activity and durability for the ORR than those of the monometallic Pt catalyst, indicating that the formation of heterostructures can provide more active catalytic surfaces. Strikingly, the ORR activities were highly dependent on the shape of the cores and the Au nanooctahedron@Pt showed the largest improvement of the ORR activity (Fig. 8).[137]

Bimetallic Pt@Ru and Ru@Pt core–shell NPs have been prepared following the dendrimer-encapsulated nanoparticle (DEN) route. By this approach, it is possible to place the desired metal preferentially either on the surface or in the core of the particles by adjusting the NP synthesis path. The presence of Ru improved the catalytic performance in the CO_{ad} electro-oxidation reaction in relation to Pt-only species. The best results were obtained for the sample with a Pt-enriched surface, where it combined the advantages resulting from the presence of Ru with a better stability due to its preferential location in the core of the NP.[138] Eichhorn, Mavrikakis and colleagues have systematically

 This journal is © The Royal Society of Chemistry 2011

Downloaded by University of Science and Technology of China on 06/05/2013 14:52:51.
Published on 08 August 2011 on http://pubs.rsc.org | doi:10.1039/C1JM12020D

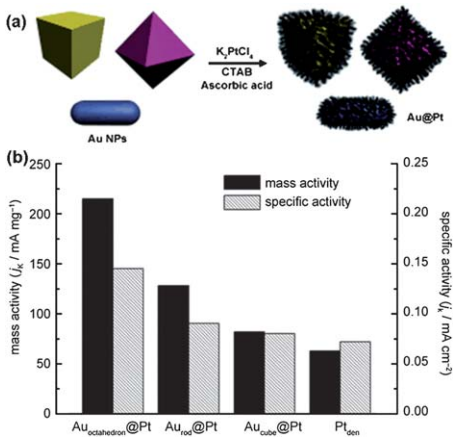

Fig. 8 (a) Schematic synthesis of AuPt bimetallic heteronanostructures consisting of Au nanocrystal cores with well-defined morphologies and dendritic shells of Pt. (b) Mass- and area-specific activity at 0.8 V *versus* RHE (reversible hydrogen electrode) for the various nanocatalysts toward ORR. Adapted with permission from ref. 137. Copyright 2010, Wiley-VCH Verlag GmbH & Co. KGaA.

studied Pt-based NPs for PROX reaction. They reported a first-principles-guided synthesis of Ru@Pt NPs with an approximately 1–2-monolayer-thick shell of Pt atoms. The distinct catalytic properties of these well-characterized core-shell NPs were demonstrated for PROX in hydrogen feeds and subsequent hydrogen light-off. For H_2 streams containing 1000 ppm CO, H_2 light-off was completed by 30 °C, significantly better than that over PtRu nanoalloys (85 °C), monometallic mixtures of NPs (93 °C) and pure Pt particles (170 °C). Density functional theory studies suggested that the enhanced catalytic activity for the core–shell NP originated from a combination of an increased availability of CO-free Pt surface sites on the Ru@Pt NPs and a hydrogen-mediated low-temperature CO oxidation process that was clearly distinct from the traditional bifunctional CO oxidation mechanism.[139] They have also prepared Rh@Pt core–shell, RhPt (1 : 1) alloy, and Rh + Pt monometallic NPs and employed Al_2O_3 as a support for them with 1.0 wt% Pt loading. The supported catalysts with three different architectures were evaluated for the PROX reaction. For hydrogen feeds with 0.2% CO and 0.5% O_2, the Rh@Pt NP catalyst had the best activity with complete CO oxidation at 70 °C and very high PROX selectivity at 40 °C with 50% CO conversion, which was much higher than that over Pt + Rh and PtRh alloy catalysts (Fig. 9).[140] Recently, they have combined first-principles calculations and experiments to systematically investigate the PROX reactivity of specifically synthesized and characterized M@Pt NPs, made of various transition metal cores (Ru, Rh, Ir, Pd, Au) covered by a *ca.* 1–2 monolayer thick shell of Pt atoms. Among these NPs, the PROX reactivity was the highest for Ru@Pt core–shell NPs, where the CO oxidation was complete by 30 °C (1000 ppm CO in H_2), followed by Rh@Pt, Ir@Pt, Pd@Pt, pure Pt, and Au@Pt NPs, in order of decreasing activity. Both the PROX activity and selectivity of several of these M@Pt core–shell NPs were significantly improved compared to monometallic and bulk nonsegregated bimetallic nanoalloys.[141]

Xia's group has synthesized Pd–Pt bimetallic nanodendrites consisting of a dense array of Pt branches on a Pd core by

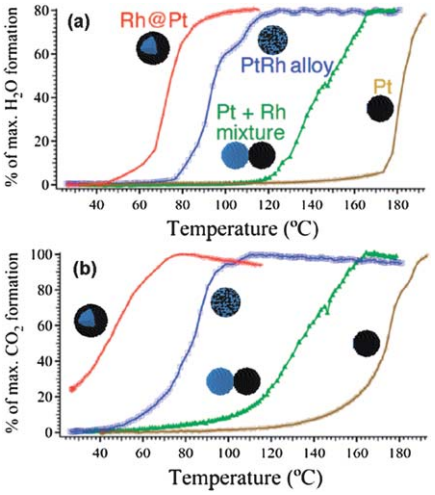

Fig. 9 Temperature-programmed reaction (TPR) plots showing (a) H_2O formation and (b) CO_2 formation for monometallic Pt NPs, monometallic mixtures of Pt NPs, and 2.7 nm Rh particles, 4.9 nm $Pt_{50}Rh_{50}$ alloy NPs, and 3.2 nm Rh@Pt NPs for H_2 streams contaminated with 2000 ppm CO. Percent of maximum H_2O formation was calculated from the limiting reactant, O_2, and % of maximum CO_2 formation is relative to the CO inlet concentration. Adapted with permission from ref. 140. Copyright 2008, American Chemical Society.

reducing K_2PtCl_4 with L-ascorbic acid in the presence of uniform Pd nanocrystal seeds in an aqueous solution. The results indicated that both homogeneous and heterogeneous nucleation of Pt occurred at very early stages of the synthesis and the growth proceeded *via* particle attachment. The Pd seeds played a crucial role in forming an open, dendritic structure by providing multiple nucleation sites for Pt that were spatially separated from each other, helping to avoid overlap and fusion between the Pt branches during the growth process. In contrast, extensive self-aggregation of small Pt particles led to the formation of Pt nanostructures with a foam-like morphology in the absence of Pd seeds. The Pt branches supported on faceted Pd nanocrystals exhibited relatively large surface areas and particularly active facets toward formic acid oxidation and the ORR, in the latter of which the Pd–Pt nanodendrites were 2.5 times more active on the basis of equivalent Pt mass for the ORR than the state-of-the-art

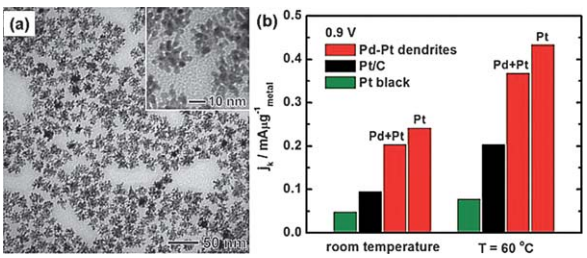

Fig. 10 (a) TEM image of Pd–Pt nanodendrites synthesized by reducing K_2PtCl_4 with L-ascorbic acid in the presence of truncated octahedral Pd nanocrystal seeds in an aqueous solution. The inset shows an enlarged image. (b) Specific activity at 0.9 V *versus* RHE for Pd–Pt dendrites, Pt/C and Pt black catalysts towards ORR reaction. Adapted with permission from ref. 142. Copyright 2009, American Association for the Advancement of Science.

Downloaded by University of Science and Technology of China on 06/05/2013 14:52:51.
Published on 08 August 2011 on http://pubs.rsc.org | doi:10.1039/C1JM12020D

Pt/C catalyst and 5 times more active than the first-generation supportless Pt-black catalyst (Fig. 10).[142,143]

3.3 Core–shell NPs combining noble and non-noble metals

The combination of Pt and another non-noble metal has intensive studies among bimetallic core–shell NPs. Zhou *et al.* have synthesized the reciprocal core–shell structured NPs, Pt@Cu and Cu@Pt, and made the preliminary evaluation of γ-Al_2O_3 supported NPs for catalytic NO reduction. Results showed that the Cu@Pt NPs had high activity equal to that of pure Pt NPs but with significantly greater selectivity for N_2 formation. The origin of the enhanced performance of the Cu@Pt was tentatively explained to be related to near surface alloy (NSA) effects, in which subsurface metal layer effects the binding of adsorbates (*e.g.* NO and H) to the particle surface.[144] The Cu@Pt/C catalyst was synthesized by sequential reduction of cupric chloride and chloro-platinic acid by using ascorbic acid, followed by anchoring on H_2O_2-functionalized Vulcan XC-72. The cyclic voltammogram results showed that formation of Pt in the form of a shell on Cu species helped to improve the reactive surface area as the skin layer adopting the surface geometric features of the core material. The electrocatalytic activities of the ORR for Cu@Pt/C catalyst had more positive onset potential than that of conventional Pt_{20}, underlining the fact that the core–shell structured catalyst was more efficient for ORR.[145] Similarly, sub-10 nm Ni@Pt core–shell NPs with near monolayer Pt shells were fabricated by a modified polyol process. Characterization results indicated that the deposition of the Pt shell could result in a lattice expansion of the Ni core and the electrochemical responses of these particles revealed that they had a Pt surface with a compressively strained Pt–Pt interatomic distance as compared to that in pure Pt NPs. The specific activity for the ORR on the Ni@Pt NPs was significantly higher than that on pure Pt particles, indicating that the Ni@Pt NPs could be promising catalysts for the cathodes of PEM fuel cells with much reduced Pt content but significantly increased catalytic activity.[146] A carbon supported core–shell PtNi@Pt NP catalyst was synthesized through a two-step solution-phase reduction method, and it demonstrated a 5.4 times higher specific activity of ORR than a conventional Pt/C catalyst by using a rotating disk electrode in a three-compartment electrochemical cell, which could be attributed to the modified electronic structure of the Pt surface layer by the underlying Ni sublayer.[147] Yang *et al.* reported carbon supported M@Pt (M = Ni, Co) core–shell NPs with uniform dispersion of diameters of 2–4 nm by a polyol synthesis process with oleic acid as the surfactant. The M@Pt/C catalysts were used for hydrogen generation from hydrolysis of ammonia borane and showed favorable performances, delivering a high hydrogen release rate of 5469 mL min^{-1} g^{-1} and 4874 mL min^{-1} g^{-1}, respectively for $Ni_{0.33}$@$Pt_{0.67}$/C and $Co_{0.32}$@$Pt_{0.68}$/C, both of which were higher than that of a monometallic NP catalyst.[148,149] Our group has synthesized carbon-supported Fe@Pt NPs using a sequential reduction process. The Fe core was first synthesized by reduction of $FeSO_4$ using $NaBH_4$ in an aqueous solution with well-dispersed carbon in the presence or absence of NH_3BH_3 in air at room temperature, respectively affording amorphous and crystalline Fe NPs. Then the atoms in the outer layer of the Fe core were sacrificed to reduce Pt^{2+} to form the Pt shell. Unexpectedly, in contrast to its crystallized counterpart, iron in the amorphous state exerted a distinct and powerful ability as a core for the Fe@Pt NPs, which combined high catalytic activity, low cost, long-term stability and easy recovery. The resultant amorphous Fe core-based Fe@Pt NPs were far more active for NH_3BH_3 oxidation (up to 354%) than the commercial Pt/C catalysts (Fig. 11).[150]

The Au@Co core–shell NPs with ~7 nm sizes obtained by one-step reduction method in our group, which we mentioned above, showed significant synergistic effects in heterogeneous catalysis. The catalytic properties of Au@Co NPs with those of pure Au, Co and AuCo alloy NPs were evaluated for dehydrogenation of aqueous NH_3BH_3. The Au@Co NPs exhibited markedly high catalytic activity to complete the dehydrogenation reaction of NH_3BH_3. This excellent catalytic activity was much higher than that of the AuCo alloy and Co with similar morphologies and sizes as those of Au@Co NPs. The Au NPs, which were in interlaced branch shapes with diameters less than 10 nm, had the worst activity. The better catalytic activity of Au@Co core–shell than AuCo alloy NPs might result from the modification of the electronic structure in a core–shell NP which is superior to that in an alloy NP for the dehydrogenation of aqueous NH_3BH_3.[104] The Au@Co core–shell NPs synthesized by octadecylamine reduction also showed better catalytic efficiency than pure Au or Co NPs in the CO oxidation.[106] Bifunctional catalytic and magnetic Ni@Ru core–shell NPs were synthesized most recently by means of a seeded growth method, where oleylamine was demonstrated to be a key factor for the creation of uniform Ni@Ru NPs with a jagged Ru shell. The ultra-small Ru NPs stabilized on the Ni surface showed higher activity than monometallic Ru NPs and physical mixture of Ru and Ni for catalytic dehydrogenation of aqueous NH_3BH_3.[151] The Ag@Ni core–shell NPs with a typical size of 14.9 ± 1.2 nm and a tunable shell thickness have been fabricated *via* a simple one-pot synthetic route using oleylamine as both solvent and reducing agent and triphenylphosphine as a surfactant. The as-synthesized Ag@Ni NPs exhibited excellent catalytic properties for the generation of H_2 from dehydrogenation of $NaBH_4$ in aqueous solution. The

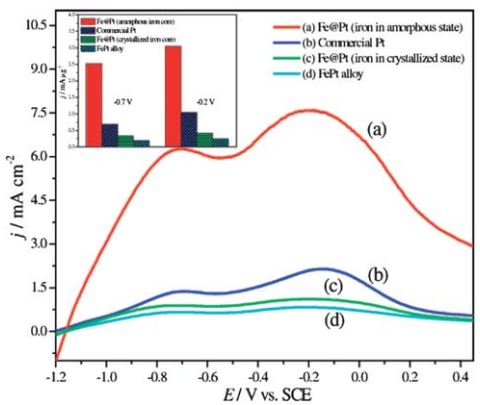

Fig. 11 Comparison of catalytic activities for NH_3BH_3 oxidation of (a) carbon supported Fe@Pt NPs with amorphous iron cores, (b) commercial Pt, (c) Fe@Pt NPs with crystallized iron cores, and (d) the FePt alloy. Electrolyte: 0.01 M NH_3BH_3/1 M NaOH; sweep rate: 10 mV s^{-1}; rotation rate: 1600 rpm; room temperature; Pt loading: 24.6 μg cm^{-2}. Inset: Comparison of the mass activities at −0.7 and −0.2 V. Reproduced with permission from ref. 150. Copyright 2009, American Chemical Society.

 This journal is © The Royal Society of Chemistry 2011

View Article Online

Downloaded by University of Science and Technology of China on 06/05/2013 14:52:51.
Published on 08 August 2011 on http://pubs.rsc.org | doi:10.1039/C1JM12020D

Table 2 Synergistic effects in catalysis over bimetallic core–shell NPs

Catalyst	NP size (nm)	Catalytic reaction	Ref.
Au@Ag/silicate sol–gel	~16	electrocatalytic reduction of H_2O_2	126
Ag@Au	4.3 ± 0.9	glucose oxidation	127
Ag@Au	~2.0	glucose oxidation	128
Ag–Au@CSs		reduction of 4-nitrophenol	129
Au@Ag/ZIF-8	3–6	reduction of 4-nitrophenol	102
Pd–Au@dendrimer	1–3	hydrogenation of allyl alcohol	130
Pd on Au	~4	trichloroethene hydrodechlorination	131
Au@Pd/Al_2O_3	2–10	direct H_2O_2 synthesis from O_2 and H_2	132
Pd@Au/TiO_2		oxidation of alcohols	133
Au@Pd/TiO_2	6.6 ± 1.2	oxidation of 1-phenylethanol by H_2O_2	134
Pt-around-Au	~2.8 + 6.1	formic acid elecrooxidation	135
Au@Pt dendritic shell	20–35	methanol electrooxidation	136
Au@Pt dendritic shell		oxygen reduction reaction	137
Pt@Ru or Ru@Pt-DEN	~2	CO electrooxidation	138
Rh@Pt	4.1	PROX in H_2-rich gas stream	139
Rh@Pt	~5	PROX in H_2-rich gas stream	140
M@Pt (M = Ru, Rh, Ir, Pd, or Au)	2–4.5	PROX in H_2-rich gas stream	141
Pd@Pt dendrites	23.5	oxygen reduction reaction	142
Pd@Pt dendrites		oxygen reduction, HCOOH electrooxidation	143
Pt@Cu and Cu@Pt	9–10 and 8–20	NO reduction	144
Cu@Pt/C	3–4	oxygen reduction reaction	145
Ni@Pt	5.0–5.4	oxygen reduction reaction	146
PtNi@Pt/C	5–8	oxygen reduction reaction	147
Ni@Pt/C	2–4	dehydrogenation of aqueous NH_3BH_3	148
Co@Pt/C	3	dehydrogenation of aqueous NH_3BH_3	149
Fe@Pt/C	~2	electrooxidation of NH_3BH_3	150
Ni@Ru/C	~15	dehydrogenation of aqueous NH_3BH_3	151
Ag@Ni	~15	dehydrogenation of aqueous $NaBH_4$	152

hydrogen generation rate of Ag@Ni NPs was found to be much higher than that of Ag and Ni NPs with similar sizes, indicating the synergistic effects between Ag and Ni.[152] Some reported bimetallic core–shell NPs with synergistic catalytic effects in catalytic reactions are summarized in Table 2.

In addition to NPs with alloy and core–shell structures, there are also some bimetallic particles with special nanostructures featuring synergistic catalytic performances. Here we give one recent example. Lu *et al.* have demonstrated bimetallic Au–Pt nanorods (NRs) to be *in situ* grown and embedded into thermosensitive core–shell microgel particles by a novel two-step approach: Au NRs pre-formed and embedded into the shell of poly(*N*-isopropylacrylamide) (PNIPA) networks, followed by Pt preferentially deposited onto the tips of Au NRs to form dumbbell-shaped bimetallic NPs. Quantitative analysis of the catalytic activity for the reduction of 4-nitrophenol indicated that bimetallic Au–Pt NRs showed highly enhanced catalytic activity due to the synergistic effect of bimetallic NPs.[153]

4. Synergistic catalysis over trimetallic and multimetallic NPs

In contrast to mono- and bi-metallic NPs, tri- and multi-metallic NPs may possess an even greater degree of catalytic activity and selectivity because more variables are available for tuning. There are limited reports but rapidly growing interest in tri- and multi-metallic NPs in the last two years. As reviewed above, Pt- and Pd-based bimetallic NPs have been intensively investigated as fuel cell catalysts. Improving efficiency and reducing overall cost are two key issues to the commercialization of fuel cell powered vehicles. The introduction of a third/fourth metal to the NP catalyst is expected to produce a combination of effects such as reduction of the lattice distance, the addition of surface sites for the formation of metal–oxygen bond and adsorption of OH^-, and the modification of the *d*-band center. In order to continuously reduce cost (by reducing the amount of Pt in the catalyst) and simultaneously increase efficiency, Pt- and/or Pd-based tri- and multi-metallic NP catalysts have also been further developed recently.

Zhong, He and coworkers have made core-shell synthesis protocol for the preparation of ternary PtMFe (M = V, Ni) NPs with a few nanometres in core sizes. The PtMFe cores were encapsulated with a shell of mixed amine/acid monolayer and microstructure observations demonstrated the composition uniformity in the individual NP. The PtMFe NPs were assembled on carbon supports with controllable dispersion and mass loading. The carbon-supported alloy NPs after calcination treatment were found to display high electrocatalytic activities for the ORR. The electrocatalytic activity data were compared for the PtVFe/C catalyst in terms of relative mass activities at 0.8 V. In comparison with a commercially available standard Pt/C catalyst (TKK), PtFe and PtVFe had relative activities almost two and four times larger than that of the commercially available Pt catalyst, respectively. The PtNiFe/C catalyst displayed a relative activity almost five times larger than that of the commercially available Pt/C catalyst. The activity displays the order of PtNiFe/C > PtVFe/C > PtFe/C > Pt/C (Fig. 12), demonstrating the effectiveness of the alloy composition in enhancing the electrocatalytic performance. The superior activity of trimetallic NPs was attributed to the alloy NPs located on the surface of the supporting carbon, whereas the traditional synthesis method may cause some NPs to occur inside the micropores of the carbon, which were not accessible by the molecular oxygen.[154–156]

Downloaded by University of Science and Technology of China on 06/05/2013 14:52:51.
Published on 08 August 2011 on http://pubs.rsc.org | doi:10.1039/C1JM12020D

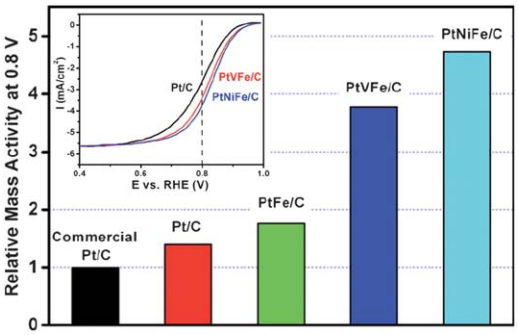

Fig. 12 Comparison of the relative electrocatalytic activities for carbon-supported monometallic, binary and ternary catalysts. Inset: RDE curves for ORR at $Pt_{32}V_{14}Fe_{54}$/C (31% metal loading), $Pt_{31}Ni_{34}Fe_{35}$/C (30% metal loading) and standard Pt/C (20% metal loading) catalysts on glassy carbon electrode (catalyst loading 15 mg, 0.196 cm^2 geometric area) in 0.5 M H_2SO_4. Scan rate: 5 mV s^{-1}, and rotating speed: 2000 rpm. Adapted with permission from ref. 156. Copyright 2008, The Royal Society of Chemistry.

Sun and coworkers have employed a two-step method for synthesizing core–shell structured Pd@FePt NPs with a 5 nm Pd core and a FePt shell whose thickness is tunable from 1 to 3 nm. The uniform FePt shell was formed by controlled nucleation of $Fe(CO)_5$ in the presence of a Pt salt and Pd NPs at designated reaction temperatures. The Pd/FePt NPs showed FePt shell-dependent catalytic properties, and those having a 1 nm coating exhibited drastic increases in durability and activity (15 times more active with a 140 mV gain in onset potential in comparison with those having a 3 nm coating).[157] Subsequently, they have designed and synthesized Au@$FePt_3$ and even Pd@Au@FePt core–shell NPs *via* epitaxial growth of FePt shell over Au and Pd@Au seeds, respectively.[130,158] The trimetallic Au@$FePt_3$ NPs possess both the high catalytic activity of Pt-bimetallic alloys and the superior durability of the tailored morphology and composition profile, with mass-activity enhancement of more than 1 order of magnitude over Pt catalysts (Fig. 13), revealing the great potential of utilizing multimetallic nanostructures in tuning the catalytic and durability properties of nanocatalysts.

Wang and Yamauchi have reported an autoprogrammed synthesis of Au@Pd@Pt triple-layered core–shell NPs, which consist of an Au core, a Pd inner layer, and a nanoporous Pt outer shell, in aqueous solution with ascorbic acid and Pluronic F127 at room temperature (Fig. 14). The proposed autoprogrammed synthesis was performed by spontaneous step-by-step depositions of metal precursors without the need for any additional and complex treatments, where the pre-formed Au NPs served as *in situ* seeds for the subsequent depositions of the Pd inner layer and the Pt outer shell, in tandem. After the formation of Au@Pd core–shell NPs, Pt deposited onto the surface of the Au@Pd binary core. With continuous Pt reduction by ascorbic acid, Pt atomic addition continuously occurred, resulting in the continuous growth of the intermediate Pt outer shell, and then more and more Pt nanoarms grew from the Au@Pd binary core surface. It was assumed that the Pluronic F127 served as a structure-directing agent to direct the nanodendritic Pt outer shell growth during the later Pt deposition. The resultant Au@Pd@Pt triple-layered NPs showed higher catalytic performance than that of Au@Pt core–shell NPs in the methanol oxidation reaction.[109] Most recently,

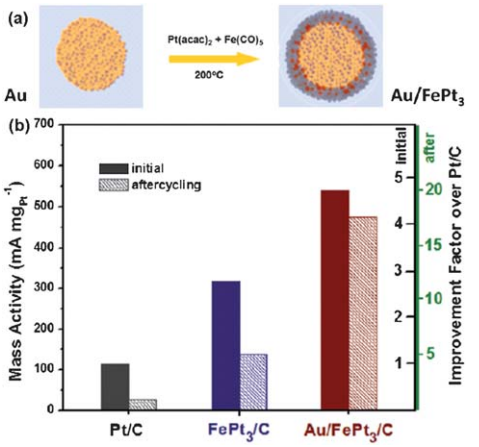

Fig. 13 (a) Schematic illustration for Au@$FePt_3$ core–shell NP synthesis. (b) Mass activities (normalized by the initial loading of Pt metal) of the Pt/C, $FePt_3$/C, and Au@$FePt_3$/C catalysts by 60000 potential cycles between 0.6 and 1.1 V *vs.* RHE in oxygen saturated 0.1 M $HClO_4$ electrolyte at 20 °C with a sweep rate of 50 mV s^{-1}. Adapted with permission from ref. 158. Copyright 2011, American Chemical Society.

Tian and coworkers have synthesized Au@Pd@Pt NPs using the atomic radius, cohesive energy, and electronegativity of these three metals to initiate different growth modes. Au NPs coated with two atomic layers of Pd and a half-monolayer equivalent of Pt clusters ($\theta_{Pt} \approx 0.5$) possessed the highest catalytic activity for electrooxidation of formic acid compared to other nanostructures such as Au@Pd NPs and Au@Pt NPs using massive electrodes. An increase in the loading of Pd beyond 2 atomic layers and Pt beyond $\theta_{Pt} \approx 0.5$ actually decreased catalytic activity, inferring that a synergistic effect exists between the three different nanostructure components (sphere, shell and islands).[159] Carbon-supported pseudo-core@shell PdCu@Pt NPs with intimate contact of Pt and PdCu were prepared by a galvanic displacement reaction between PdCu/C alloy NPs and $PtCl_6^{2-}$ in aqueous solution. The PdCu@Pt/C catalysts demonstrated higher specific activity to methanol oxidation and ORR than Pt/C and PtRu/C as a result of improved Pt utilization.[160] For the PdCo@Pd core–shell NPs

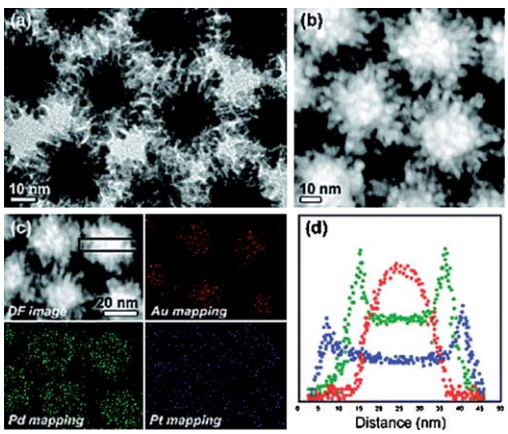

Fig. 14 (a) TEM image, (b) HAADF-STEM image, and (c) HAADF-STEM-EDS mapping images of the Au@Pd@Pt core–shell NPs. (d) Cross-sectional compositional line profiles of the square area in (c). Reproduced with permission from ref. 109. Copyright 2010, American Chemical Society.

This journal is © The Royal Society of Chemistry 2011

Downloaded by University of Science and Technology of China on 06/05/2013 14:52:51.
Published on 08 August 2011 on http://pubs.rsc.org | doi:10.1039/C1JM12020D

obtained from H_2-induced surface segregation effect (the synthesis was mentioned in Section 3.1), an ultralow loading of Pt was deposited on its surface by spontaneous displacement reaction and the Pt-decorated PdCo@Pd/C catalyst was found to have significantly enhanced stability and ORR activity. Both PdCo@Pd/C and Pt-decorated PdCo@Pd/C catalysts showed much higher MeOH tolerances than Pt/C.[120] The Pd–Pt–Ni nanoalloy catalysts have been synthesized by a polyol reduction method and characterized for the ORR in PEM fuel cells. The performance of the membrane-electrode assembly (MEA) fabricated with the Pd–Pt–Ni catalysts, with a lower cost than that of Pt, was found to increase continuously in the entire current density range with the operation time in the PEM fuel cells until it becomes comparable to that of commercial Pt. The Pt-based mass activity of Pd–Pt–Ni exceeded that of commercial Pt by a factor of 2, and its long-term durability was comparable to that of commercial Pt within the 200 h of operation. Composition analyses suggested a dealloyed active catalyst phase consisting of a Pd-rich core and a Pt-rich shell formed by dissolution of Pd and Ni under the fuel cell testing conditions. It was assumed that the strain effect caused by lattice mismatch between the Pd-rich core and the Pt-rich shell may down-shift the *d*-band center, lower the adsorption energy of surface oxygenated intermediates, and thus enhance the surface catalytic activity.[161]

In addition to electrochemical catalysis, tri- and multi-metallic NPs have also showed their synergistic effects in other types of catalytic reactions. Hungria *et al.* have discovered the synergistic value of mesoporous silica supported trimetallic NP catalyst Ru_5PtSn, derived from a heterotrinuclear (Ru–Pt–Sn) complex, as a highly efficient and selective means of effecting the catalytic single-step hydrogenation of dimethyl terephthalate (DMT) to cyclohexanedimethanol (CHDM) under mild conditions. The presence of tin in the NP catalyst was regarded to play a key role in anchoring the particle owing to its oxophilicity for the support, which in turn diminished the tendency for the sintering of NPs.[162] The temperature-programmed oxidation of methane revealed that the addition of Pt and Au to Pd/CeO_2 catalyst resulted in higher conversion values in the whole investigated temperature range compared to the monometallic Pd catalyst. The time-on-stream experiments provided further evidence for the high-stability of tri-metallic catalysts compared to the monometallic one. It was suggested that advantageous catalytic properties of tri-metallic Pt–Au–Pd/CeO_2 catalysts compared to the monometallic one can be attributed to suppression of the formation of ionic forms of Pd(II), reaching an optimum ratio between Pd^0 and PdO species, and stabilization of Pd in high dispersion.[163] The colloidal dispersions of PVP-protected Au/Pt/Rh trimetallic NPs, assumed to have a Au-core/Pt-interlayer/Rh-shell triple-layer structure, were prepared by mixing the dispersions of PVP-protected Rh NPs and those of PVP-protected bimetallic $Au_1@Pt_4$ core–shell NPs. The trimetallic NPs with the composition of Au/Pt/Rh (1/4/20) and a triple core–shell structure had the highest catalytic activity for hydrogenation of methyl acrylate at 30 °C in ethanol among the trimetallic NPs with other compositions and other structures, and the corresponding mono- and bi-metallic NPs (Fig. 15). The high catalytic activity of trimetallic NPs could be due to the sequential electronic effect between elements in a particle and the strong exothermic interaction could be the driving force for the self-organization to form the triple core–shell structure.[164] Following the similar physical mixing method, the same group also reported polymer-protected Pd/Ag/Rh triple-layered core–shell trimetallic NPs by mixing dispersions of polymer-protected Rh NPs and Pd@Ag core–shell NPs. The spontaneously formed trimetallic NPs having an atomic composition of Pd/Ag/Rh = 1/2/13.5 and an average diameter of 2.2 nm showed the highest catalytic activity among the metal NP catalysts for hydrogenation of methyl acrylate at 30 °C under an atmosphere of hydrogen.[165]

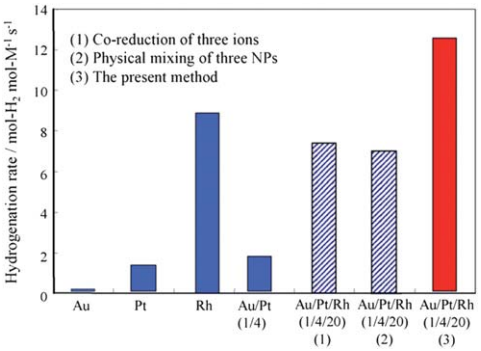

Fig. 15 Comparison of catalytic activities of various metal NPs for hydrogenation of methyl acrylate. Reproduced with permission from ref. 164. Copyright 2007, Elsevier.

Table 3 Synergistic effects in catalysis over tri- and multi-metallic NPs

Catalyst	NP size (nm)	Catalytic reaction	Ref.
PtMFe/C (M = Ni, V)	~2	oxygen reduction reaction	156
Pd@FePt	~6	oxygen reduction reaction	157
$Au@FePt_3$	~10	oxygen reduction reaction	158
Au@Pd@Pt	~35	methonal electrooxidation	109
Au@Pd@Pt	55	formic acid electrooxidation	159
PdCu@Pt/C	~4.3	MeOH electrooxidation, oxygen reduction	160
Pt-doped PdCo@Pd/C		oxygen reduction reaction	120
Pd–Pt–Ni	5	oxygen reduction reaction	161
Ru_5PtSn/SiO_2		hydrogenation of dimethyl terephthalate to cyclohexanedimethanol	162
Pt–Pd–Au/CeO_2		methane total oxidation	163
Au@Pt@Rh	~3	hydrogenation of methyl acrylate	164
Pd@Ag@Rh	~3.5	hydrogenation of methyl acrylate	165
Au/Ag/Pd	4.2 ± 0.5	Sonogashira C–C coupling	166
Au–Ag–Pd	13 ± 0.5	Suzuki C–C coupling	167
Pd–Bi–Au/C	13	oxidation of polyethylene glycol dodecyl ether	168

Downloaded by University of Science and Technology of China on 06/05/2013 14:52:51.
Published on 08 August 2011 on http://pubs.rsc.org | doi:10.1039/C1JM12020D

The Au/Ag/Pd trimetallic NPs and Pd NPs were synthesized by a chemical method with CTAB as the capping agent. The catalytic activities of Pd and the trimetallic NPs were examined for the Sonogashira and Suzuki C–C coupling reactions. Results showed that the trimetallic Au/Ag/Pd NPs with 1/1/1 ratio exhibited better catalysis than Pd NPs in both reactions, which may be due to the concerted electronic effects among these metal atoms.[166,167] Zhou *et al.* have prepared onion-like Pd–Bi–Au/C catalyst particles with an average diameter of 13 nm by consecutive chemical reduction of Au, Bi and Pt precursors in aqueous solution and immobilization on active carbon. The onion-like morphology was composed of high content of Au inner core, Bi-rich intermediate layer and Pd-rich external layer based on characterization data. The Pd–Bi–Au/C trimetallic catalyst demonstrated good catalytic properties for the oxidation of polyethylene glycol dodecyl ether in liquid phase using water as solvent and O_2 as oxidant at atmospheric pressure, superior to a traditional bimetallic Pd–Au/C catalyst. It indicated that Bi, as promoter element, may play an important role in the electronic interaction of Pd and Au NPs.[168] Some reported tri- and multi-metallic NPs with synergistic catalytic effects in respective catalytic reactions are summarized in Table 3.

5. Conclusion and outlook

This feature article has provided a survey of development of bi- and tri-metallic, even multimetallic NPs for synergistic catalysis studies in the last 5–6 years. We have tried to present an up-to-date overview in such a rapidly growing field, while the subject is very active and many papers are contributed each year (even during the writing of this article) from chemists, physical and materials scientists, *etc.* Therefore, it is hard to take into account all publications to this field in limited pages. We apologize here if some significant contributions were left out.

Bimetallic alloy NPs have been widely developed with improved catalytic activity. For core–shell structured bimetallic NPs, we have introduced some fabrication strategies, including typical successive reduction or seeded/epitaxial growth, one-step reduction, galvanic replacement reaction, surface phase segregation, physical mixing, and so on. The core–shell NPs usually have significantly higher activities than the monometallic counterparts, even alloy NPs. In recent years, the development of tri- and multi-metallic NPs for catalysis, especially electrochemical catalysis, is becoming a very hot topic. The combination of relatively cheap components with less noble metal into one catalyst affords more opportunities to lower cost and improve catalytic efficiency.

It is worthy to note here that it could be untimely to generalize which structure or which combination is definitely better for a catalytic reaction. For example, we may find many bimetallic NPs with core–shell structure having higher catalytic activities than those of alloyed structure,[104,139–141,150] whereas the AuAg alloy NPs are especially active for CO oxidation reaction,[32–36] in which Au adsorbs CO molecules and the neighbouring Ag species adsorbs and affords reactive oxygen, thus greatly facilitating the reaction process. Therefore, different reactions have their special requirements for catalyst structure, composition and combination, that is, case by case. With the development of synthetic techniques, desired structures and various composition combinations, which are currently unrealized, could be fabricated to improve the catalytic properties.

The synergistic catalytic effect over heterometallic NPs based on the reports mentioned in this article could be tentatively ascribed to the following main aspects. 1) Improved activity results from microstructure changes of nanocatalyst upon introducing another metal species. 2) In many cases, electronic interaction among the different components along with geometric effects leads to appropriate modification of electronic structure, which benefits the catalytic activity enhancement. 3) Among many bimetallic ($metal_A$ and $metal_B$) nanocatalysts, although $metal_B$ is less active or inactive for the reaction, the addition of $metal_B$ to $metal_A$ can effectively improve the entire activity of the bimetallic NPs by its "indirect" function. For example, the presence of Rh increases the thermal stability of PtRh–BHA catalyst;[52] the Sn prevents sintering in RuPtSn NPs;[162] the presence of Au reduces the poisoning of AuPd NPs;[25] the Au is resistant to oxidation of AuAg NPs;[37] $metal_B$ helps to activate the catalytic substrate molecules;[32–34,79] $metal_B$ leads to the better dispersion of $metal_A$;[67,68,80] *etc.* 4) Among the competitive reactions, the predominant reaction is changed from pathway A to desirable pathway B upon alloying, thus improving the catalytic activity.[60,83,84] 5) Other reasons. It should be pointed out that more than one of the aspects summarized above could exist in one heterometallic catalyst for its enhanced catalytic efficiency.

Although great progress has been achieved, some problems still need to be faced. The present heterometallic NP catalysts are mostly based on noble metals. The high cost and scarce availability make the industrialization very difficult. Further efforts should be made to develop much more effective and economical catalysts. As one vivid example, a family of non-noble metal catalysts, derived from polyaniline, Fe, and Co, as an inexpensive alternative was just reported that approached the performance of Pt-based systems at a cost sustainable for high-power fuel cell applications.[169] On the other hand, researchers working in the catalysis field are more concerned about catalytic performance and only some groups carefully investigate the catalyst microstructures. Sometimes, there are even no morphology and size characterizations for metal NP catalysts in some reports. It is important to construct the relationship between catalyst structure and performance, so that we can understand how to modify the preparation conditions to obtain "desirable" catalysts with improved activity. Materials chemists, being good at materials synthesis, full characterizations and understanding of formation mechanisms for the catalysts, develop novel catalysts while they usually prefer some model reactions to test the performance of the catalysts, where some superior catalysts are possibly overlooked for important industrial applications. Therefore, extensive collaborations among synthetic, materials chemists and scientists in the catalysis field could bridge/compensate for such gaps/losses and make the research go one step further. In addition, although theoretical works were not involved in this article, first principles calculations might help to guide the composition choice for the intelligent design of catalysts in experimental works, and also afford microscopic insights into the fundamental factors underlying their activity.

Along with the development of materials science at an extraordinary pace, we may be able to synthesize heterometallic NPs with experimentally controllable size, composition and

 This journal is © The Royal Society of Chemistry 2011

View Article Online

chemical ordering under suitable reaction conditions, choice of precursor materials, and combining physical, chemical, and even biological generation methods. The advanced characterizations will pave the way for making clear the relationship between the precise microstructure of heterometallic NPs and their catalytic performance. We have reason to believe that the foreseeable future in this field will be very bright.

Acknowledgements

We are grateful to JSPS and AIST for the financial support. H.L.J. thanks JSPS for a postdoctoral fellowship. The authors thank Mr Lei Deng and Dr Gang Xu for their kind help in preparing the graphical abstract image.

Downloaded by University of Science and Technology of China on 06/05/2013 14:52:51.
Published on 08 August 2011 on http://pubs.rsc.org | doi:10.1039/C1JM12020D

Notes and references

1 R. L. Johnston, *Atomic and Molecular Clusters*, Taylor and Francis, London, 2002.
2 M. Haruta, N. Yamada, T. Kobayashi and S. Lijima, *J. Catal.*, 1989, **115**, 301–309.
3 A. P. Alivisatos, *Science*, 1996, **271**, 933–937.
4 C. B. Murray, C. R. Kagan and M. G. Bawendi, *Annu. Rev. Mater. Sci.*, 2000, **30**, 545–610.
5 Y. Xia, P. Yang, Y. Sun, Y. Wu, B. Mayers, B. Gates, Y. Yin, F. Kim and H. Yan, *Adv. Mater.*, 2003, **15**, 353–389.
6 M. A. El-Sayed, *Acc. Chem. Res.*, 2004, **37**, 326–333.
7 X. Wang, J. Zhuang, Q. Peng and Y. D. Li, *Nature*, 2005, **437**, 121–124.
8 Y. Xia, Y. Xiong, B. Lim and S. E. Skrabalak, *Angew. Chem., Int. Ed.*, 2009, **48**, 60–103.
9 H. M. Chen, C. K. Chen, Y.-C. Chang, C.-W. Tsai, R.-S. Liu, S.-F. Hu, W.-S. Chang and K.-H. Chen, *Angew. Chem., Int. Ed.*, 2010, **49**, 5966–5969.
10 D. S. Wang and Y. D. Li, *Adv. Mater.*, 2011, **23**, 1044–1060.
11 R. Ferrando, J. Jellinek and R. L. Johnston, *Chem. Rev.*, 2008, **108**, 845–910.
12 A. Groß, *Top. Catal.*, 2006, **37**, 29–39.
13 H. C. Ham, G. S. Hwang, J. Han, S. W. Nam and T. H. Lim, *J. Phys. Chem. C*, 2010, **114**, 14922–14928.
14 D. A. Hansgen, D. G. Vlachos and J. G. Chen, *Nat. Chem.*, 2010, **2**, 484–489.
15 N. Dimitratos and L. Prati, *Gold Bull.*, 2005, **38**, 73–77.
16 D. Wang, A. Villa, F. Porta, D. Su and L. Prati, *Chem. Commun.*, 2006, 1956–1958.
17 L. Prati, A. Villa, F. Porta, D. Wang and D. Su, *Catal. Today*, 2007, **122**, 386–390.
18 A. Villa, C. Campione and L. Prati, *Catal. Lett.*, 2007, **115**, 133–136.
19 D. Wang, A. Villa, F. Porta, L. Prati and D. Su, *J. Phys. Chem. C*, 2008, **112**, 8617–8622.
20 A. Villa, N. Janjic, P. Spontoni, D. Wang, D. S. Su and L. Prati, *Appl. Catal., A*, 2009, **364**, 221–228.
21 G. Li, D. I. Enache, J. Edwards, A. F. Carley, D. W. Knight and G. J. Hutchings, *Catal. Lett.*, 2006, **110**, 7–13.
22 P. J. Miedziak, Z. Tang, T. E. Davies, D. I. Enache, J. K. Bartley, A. F. Carley, A. A. Herzing, C. J. Kiely, S. H. Taylor and G. J. Hutchings, *J. Mater. Chem.*, 2009, **19**, 8619–8627.
23 G. Li, J. Edwards, A. F. Carley and G. J. Hutchings, *Catal. Today*, 2007, **122**, 361–364.
24 X. Zhou, Y. Huang, W. Xing, C. Liu, J. Liao and T. Lu, *Chem. Commun.*, 2008, 3540–3542.
25 Y. Huang, X. Zhou, M. Yin, C. Liu and W. Xing, *Chem. Mater.*, 2010, **22**, 5122–5128.
26 R. W. J. Scott, O. M. Wilson, S.-K. Oh, E. A. Kenik and R. M. Crooks, *J. Am. Chem. Soc.*, 2004, **126**, 15583–15591.
27 W. Hou, N. A. Dehm and R. W. J. Scott, *J. Catal.*, 2008, **253**, 22–27.
28 M. Shao, H. Wang, M. Zhang, D. D. D. Ma and S.-T. Lee, *Appl. Phys. Lett.*, 2008, **93**, 243110.
29 S. Hermans, A. Deffernez and M. Devillers, *Catal. Today*, 2010, **157**, 77–82.
30 V. Abdelsayed, A. Aljarash, M. S. El-Shall, Z. A. Al Othman and A. H. Alghamdi, *Chem. Mater.*, 2009, **21**, 2825–2834.
31 B. Hu, T. Wu, K. Ding, X. Zhou, T. Jiang and B. Han, *J. Phys. Chem. C*, 2010, **114**, 3396–3400.
32 J.-H. Liu, A.-Q. Wang, Y.-S. Chi, H.-P. Lin and C.-Y. Mou, *J. Phys. Chem. B*, 2005, **109**, 40–43.
33 A.-Q. Wang, J.-H. Liu, S. D. Lin, T.-S. Lin and C.-Y. Mou, *J. Catal.*, 2005, **233**, 186–197.
34 A.-Q. Wang, C.-M. Chang and C.-Y. Mou, *J. Phys. Chem. B*, 2005, **109**, 18860–18867.
35 C.-W. Yen, M.-L. Lin, A. Wang, S.-A. Chen, J.-M. Chen and C.-Y. Mou, *J. Phys. Chem. C*, 2009, **113**, 17831–17839.
36 X. Liu, A. Wang, X. Yang, T. Zhang, C.-Y. Mou, D.-S. Su and J. Li, *Chem. Mater.*, 2009, **21**, 410–418.
37 Y. Sun and C. Lei, *Angew. Chem., Int. Ed.*, 2009, **48**, 6824–6827.
38 C. Wang, H. Yin, R. Chan, S. Peng, S. Dai and S. Sun, *Chem. Mater.*, 2009, **21**, 433–435.
39 D. Mott, J. Luo, P. N. Njoki, Y. Lin, L. Wang and C.-J. Zhong, *Catal. Today*, 2007, **122**, 378–385.
40 W. Tang, S. Jayaraman, T. F. Jaramillo, G. D. Stucky and E. W. McFarland, *J. Phys. Chem. C*, 2009, **113**, 5014–5024.
41 M. D. Obradović, A. V. Tripković and S. L. Gojković, *Electrochim. Acta*, 2009, **55**, 204–209.
42 M. Mirdamadi-Esfahani, M. Mostafavi, B. Keita, L. Nadjo, P. Kooyman and H. Remita, *Gold Bull.*, 2010, **43**, 49–56.
43 S. Zhang, Y. Shao, H.-G. Liao, J. Liu, I. A. Aksay, G. Yin and Y. Lin, *Chem. Mater.*, 2011, **23**, 1079–1081.
44 Y. Gu, G. Wu, Xiao F. Hu, D. A. Chen, T. Hansen, H.-C. zur Loye and H. J. Ploehna, *J. Power Sources*, 2010, **195**, 425–434.
45 S.-H. Chang, W.-N. Su, M.-H. Yeh, C.-J. Pan, K.-L. Yu, D.-G. Liu, J.-F. Lee and B.-J. Hwang, *Chem.–Eur. J.*, 2010, **16**, 11064–11071.
46 A. U. Nilekar, Y. Xu, J. Zhang, M. B. Vukmirovic, K. Sasaki, R. R. Adzic and M. Mavrikakis, *Top. Catal.*, 2007, **46**, 276–284.
47 Y. Shen, S. Zhang, H. Li, Y. Ren and H. Liu, *Chem.–Eur. J.*, 2010, **16**, 7368–7371.
48 L. Prati, A. Villa, C. Campione and P. Spontoni, *Top. Catal.*, 2007, **44**, 319–324.
49 T. A. Yamamoto, T. Nakagawa, S. Seino and H. Nitani, *Appl. Catal., A*, 2010, **387**, 195–202.
50 S. T. Christensen, H. Feng, J. L. Libera, N. Guo, J. T. Miller, P. C. Stair and J. W. Elam, *Nano Lett.*, 2010, **10**, 3047–3051.
51 B. Yoon, H.-B. Pan and C. M. Wai, *J. Phys. Chem. C*, 2009, **113**, 1520–1525.
52 A. Cao and G. Veser, *Nat. Mater.*, 2010, **9**, 75–81.
53 Z. Wang, L. Wang, S. Chen, P. Zhang, J. Xu and J. Chen, *Int. J. Hydrogen Energy*, 2010, **35**, 8862–8867.
54 C.-L. Lee, C.-M. Tseng, R.-B. Wu, C.-C. Wu and S.-C. Syu, *Electrochim. Acta*, 2009, **54**, 5544–5547.
55 V. K. Tzitzios, V. Georgakilas and T. N. Angelidis, *J. Chem. Technol. Biotechnol.*, 2005, **80**, 699–704.
56 L. Liu, X. Guan, Z. Li, X. Zi, H. Dai and H. He, *Appl. Catal., B*, 2009, **90**, 1–9.
57 R. B. Biniwale, N. Kariya and M. Ichikawa, *Catal. Lett.*, 2005, **105**, 83–87.
58 A. Martins, J. M. Silva, F. R. Ribeiro and M. F. Ribeiro, *Catal. Lett.*, 2006, **109**, 83–87.
59 N. H. H. A. Bakarb, M. M. Bettahar, M. A. Bakar, S. Monteverdi, J. Ismail and M. Alnot, *J. Catal.*, 2009, **265**, 63–71.
60 S. K. Singh and Q. Xu, *Inorg. Chem.*, 2010, **49**, 6148–6152.
61 P. S. Dimick, R. G. Herman and C. E. Lyman, *Chem. Lett.*, 2010, **138**, 148–154.
62 R. Mu, Q. Fu, H. Xu, H. Zhang, Y. Huang, Z. Jiang, S. Zhang, D. Tan and X. Bao, *J. Am. Chem. Soc.*, 2011, **133**, 1978–1986.
63 L. Borkó and L. Guczi, *Top. Catal.*, 2006, **39**, 35–43.
64 E.-Y. Ko, E. D. Park, H. C. Lee, D. Lee and S. Kim, *Angew. Chem., Int. Ed.*, 2007, **46**, 734–737.
65 Y. Li, Z.-G. Li and R.-X. Zhou, *J. Mol. Catal. A: Chem.*, 2008, **279**, 140–146.
66 S. Shen, J. Zhuang, Y. Yang and X. Wang, *Nanoscale*, 2011, **3**, 272–279.
67 P. V. Samant, M. F. R. Pereira and J. L. Figueiredo, *Catal. Today*, 2005, **102–103**, 183–188.
68 M. S. Kumar, D. Chen, A. Holmen and J. C. Walmsley, *Catal. Today*, 2009, **142**, 17–23.

View Article Online

Downloaded by University of Science and Technology of China on 06/05/2013 14:52:51.
Published on 08 August 2011 on http://pubs.rsc.org | doi:10.1039/C1JM12020D

69 C. Jeyabharathi, J. Mathiyarasu and K. L. N. Phani, *J. Appl. Electrochem.*, 2009, **39**, 45–53.
70 X. Ji, K. T. Lee, R. Holden, L. Zhang, J. Zhang, G. A. Botton, M. Couillard and L. F. Nazar, *Nat. Chem.*, 2010, **2**, 286–293.
71 M. H. Pinzón, A. Centeno and S. A. Giraldo, *Appl. Catal., A*, 2006, **302**, 118–126.
72 X. Liu, A. Wang, X. Wang, C.-Y. Mou and T. Zhang, *Chem. Commun.*, 2008, 3187–3189.
73 X. Liu, A. Wang, T. Zhang, D.-S. Su and C.-Y. Mou, *Catal. Today*, 2011, **160**, 103–108.
74 C. L. Bracey, P. R. Ellis and G. J. Hutchings, *Chem. Soc. Rev.*, 2009, **38**, 2231–2243 and references therein.
75 H.-L. Jiang, S. K. Sing, J.-M. Yan, X.-B. Zhang and Q. Xu, *ChemSusChem*, 2010, **3**, 541–549.
76 H.-L. Jiang and Q. Xu, *Catal. Today*, 2011, **170**, 56–63.
77 T. Umegaki, J.-M. Yan, X.-B. Zhang, H. Shioyama, N. Kuriyama and Q. Xu, *Int. J. Hydrogen Energy*, 2009, **34**, 2303–2311.
78 H.-L. Jiang, T. Umegaki, T. Akita, X.-B. Zhang, M. Haruta and Q. Xu, *Chem.–Eur. J.*, 2010, **16**, 3132–3137.
79 M. A. Keane, S. Gómez-Quero, F. Cárdenas-Lizana and W. Shen, *ChemCatChem*, 2009, **1**, 270–278.
80 J. Zhou, L. Guo, X. Guo, J. Mao and S. Zhang, *Green Chem.*, 2010, **12**, 1835–1843.
81 H. Zhang, A. Zhu, X. Wang, Y. Wang and C. Shi, *Catal. Commun.*, 2007, **8**, 612–618.
82 R. Wojcieszak, S. Monteverdi, J. Ghanbaja and M. M. Bettahar, *J. Colloid Interface Sci.*, 2008, **317**, 166–174.
83 S. K. Singh and Q. Xu, *J. Am. Chem. Soc.*, 2009, **131**, 18032–18033.
84 S. K. Singh and Q. Xu, *Chem. Commun.*, 2010, **46**, 6545–6547.
85 A. Śrębowata, M. Sadowska, W. Juszczyk, Z. Kaszkur, Z. Kowalczyk, M. Nowosielska and Z. Karpiński, *Catal. Commun.*, 2007, **8**, 11–15.
86 J.-Q. Du, Y. Zhang, T. Tian, S.-C. Yan and H.-T. Wang, *Mater. Res. Bull.*, 2009, **44**, 1347–1351.
87 E. B. Pereira, N. Homs, S. Martí, J. L. G. Fierro and P. R. de la Piscina, *J. Catal.*, 2008, **257**, 206–214.
88 J. A. Z. Pieterse, G. Mul, I. Melian-Cabrera and R. W. van den Brink, *Catal. Lett.*, 2005, **99**, 41–44.
89 Y. Zhang, W. Huang, S. E. Habas, J. N. Kuhn, M. E. Grass, Y. Yamada, P. Yang and G. A. Somorjai, *J. Phys. Chem. C*, 2008, **112**, 12092–12095.
90 J. Bian, M. Xiao, S.-J. Wang, Y.-X. Lu and Y.-Z. Meng, *Appl. Surf. Sci.*, 2009, **255**, 7188–7196.
91 J. Bian, M. Xiao, S. J. Wang, Y. X. Lu and Y. Z. Meng, *Catal. Commun.*, 2009, **10**, 1529–1533.
92 J. Bian, M. Xiao, S. J. Wang, Y. X. Lu and Y. Z. Meng, *Chin. Chem. Lett.*, 2009, **20**, 352–355.
93 A.-G. Boudjahem, M. Chettibi, S. Monteverdi and M. M. Bettahar, *J. Nanosci. Nanotechnol.*, 2009, **9**, 3546–3554.
94 A. L. Kustov, A. M. Frey, K. E. Larsen, T. Johannessen, J. K. Nørskov and C. H. Christensen, *Appl. Catal., A*, 2007, **320**, 98–104.
95 J.-M. Yan, X.-B. Zhang, S. Han, H. Shioyama and Q. Xu, *J. Power Sources*, 2009, **194**, 478–481.
96 J. Wang, X. C. Zeng, in *Core-Shell Magnetic Nanoclusters in Nanoscale Magnetic Materials and Applications*, ed. J. P. Liu, E. Fullerton, O. Gutfleisch and D. J. Sellmyer, Springer Science & Business Media, Inc., 2009, pp. 35–65.
97 B. Lim, H. Kobayashi, T. Yu, J. Wang, M. J. Kim, Z.-Y. Li, M. Rycenga and Y. Xia, *J. Am. Chem. Soc.*, 2010, **132**, 2506–2507.
98 M. Tsuji, D. Yamaguchi, M. Matsunaga and M. J. Alam, *Cryst. Growth Des.*, 2010, **10**, 5129–5135.
99 M. Tsuji, M. Ogino, M. Matsunaga, N. Miyamae, R. Matsuo, M. Nishio and M. J. Alam, *Cryst. Growth Des.*, 2010, **10**, 4085–4090.
100 A. Sánchez-Iglesias, E. Carbó-Argibay, A. Glaria, B. Rodríguez-González, J. Pérez-Juste, I. Pastoriza-Santos and L. M. Liz-Marzán, *Chem.–Eur. J.*, 2010, **16**, 5558–5563.
101 H.-L. Jiang and Q. Xu, *Chem. Commun.*, 2011, **47**, 3351–3370.
102 H.-L. Jiang, T. Akita, T. Ishida, M. Haruta and Q. Xu, *J. Am. Chem. Soc.*, 2011, **133**, 1304–1306.
103 V. Mazumder, M. Chi, K. L. More and S. Sun, *Angew. Chem., Int. Ed.*, 2010, **49**, 9368–9372.
104 J.-M. Yan, X.-B. Zhang, T. Akita, M. Haruta and Q. Xu, *J. Am. Chem. Soc.*, 2010, **132**, 5326–5327.
105 H.-L. Jiang, T. Akita and Q. Xu, submitted for publication.
106 D. S. Wang and Y. D. Li, *J. Am. Chem. Soc.*, 2010, **132**, 6280–6281.
107 X. Huang, H. Wu, S. Pu, W. Zhang, X. Liao and B. Shi, *Green Chem.*, 2011, **13**, 950–957.
108 Y. W. Lee, M. Kim, Z. H. Kim and S. W. Han, *J. Am. Chem. Soc.*, 2009, **131**, 17036–17037.
109 L. Wang and Y. Yamauchi, *J. Am. Chem. Soc.*, 2010, **132**, 13636–13638.
110 K. J. Carroll, D. M. Hudgins, S. Spurgeon, K. M. Kemner, B. Mishra, M. I. Boyanov, L. W. Brown, III, M. L. Taheri and E. E. Carpenter, *Chem. Mater.*, 2010, **22**, 6291–6296.
111 X. Lu, J. Chen, S. E. Skrabalak and Y. N. Xia, *Proc. Inst. Mech. Eng., Part N: J. Nanoeng. Nanosyst.*, 2008, **221**, 1–16.
112 W.-R. Lee, M. G. Kim, J.-R. Choi, J.-I. Park, S. J. Ko, S. J. Oh and J. Cheon, *J. Am. Chem. Soc.*, 2005, **127**, 16090–16097.
113 Y. Lu, Y. Zhao, L. Yu, L. Dong, C. Shi, M.-J. Hu, Y.-J. Xu, L.-P. Wen and S.-H. Yu, *Adv. Mater.*, 2010, **22**, 1407–1411.
114 Y. Khalavka, J. Becker and C. Sönnichsen, *J. Am. Chem. Soc.*, 2009, **131**, 1871–1875.
115 L. Kuai, S. Wang and B. Geng, *Chem. Commun.*, 2011, **47**, 6093.
116 Q. Zhang, J. Xie, J. Y. Lee, J. Zhang and C. Boothroyd, *Small*, 2008, **4**, 1067–1071.
117 H. Kobayashi, M. Yamauchi, H. Kitagawa, Y. Kubota, K. Kato and M. Takata, *J. Am. Chem. Soc.*, 2010, **132**, 5576–5577.
118 C. Wang, S. Peng, R. Chan and S. Sun, *Small*, 2009, **5**, 567–570.
119 K. J. J. Mayrhofer, V. Juhart, K. Hartl, M. Hanzlik and M. Arenz, *Angew. Chem., Int. Ed.*, 2009, **48**, 3529–3531.
120 D. Wang, H. L. Xin, Y. Yu, Ho Wang, E. Rus, D. A. Muller and H. D. Abruña, *J. Am. Chem. Soc.*, 2010, **132**, 17664–17666.
121 F. Tao, M. E. Grass, Y. Zhang, D. R. Butcher, J. R. Renzas, Z. Liu, J. Y. Chung, B. S. Mun, M. Salmeron and G. A. Somorjai, *Science*, 2008, **322**, 932–934.
122 N. Toshima, *Macromol. Symp.*, 2008, **270**, 27–39 and references therein.
123 Y.-T. Kim, H. Lee, H.-J. Kim and T.-H. Lim, *Chem. Commun.*, 2010, **46**, 2085–2087.
124 J. Zhang, Y. Tang, L. Weng and M. Ouyang, *Nano Lett.*, 2009, **9**, 4061–4065.
125 J. Yang, E. Sargent, S. Kelley and J. Y. Ying, *Nat. Mater.*, 2009, **8**, 683–689.
126 S. Manivannan and R. Ramaraj, *J. Chem. Sci.*, 2009, **121**, 735–743.
127 S. Tokonami, N. Morita, K. Takasaki and N. Toshima, *J. Phys. Chem. C*, 2010, **114**, 10336–10341.
128 H. Zhang, J. Okuni and N. Toshima, *J. Colloid Interface Sci.*, 2011, **354**, 131–138.
129 S. Tang, S. Vongehr and X. Meng, *J. Mater. Chem.*, 2010, **20**, 5436–5445.
130 R. W. J. Scott, O. M. Wilson, S.-K. Oh, E. A. Kenik and R. M. Crooks, *J. Am. Chem. Soc.*, 2004, **126**, 15583–15591.
131 M. O. Nutt, K. N. Heck, P. Alvarez and M. S. Wong, *Appl. Catal., B*, 2006, **69**, 115–125.
132 B. E. Solsona, J. K. Edwards, P. Landon, A. F. Carley, A. Herzing, C. J. Kiely and G. J. Hutchings, *Chem. Mater.*, 2006, **18**, 2689–2695.
133 D. I. Enache, J. K. Edwards, P. Landon, B. Solsona-Espriu, A. F. Carley, A. A. Herzing, M. Watanabe, C. J. Kiely, D. W. Knight and G. J. Hutchings, *Science*, 2006, **311**, 362–365.
134 A. J. Frank, J. Rawski, K. E. Maly and V. Kitaev, *Green Chem.*, 2010, **12**, 1615–1622.
135 S. Zhang, Y. Shao, G. Yin and Y. Lin, *Angew. Chem., Int. Ed.*, 2010, **49**, 2211–2214.
136 H. Ataee-Esfahani, L. Wang, Y. Nemoto and Y. Yamauchi, *Chem. Mater.*, 2010, **22**, 6310–6318.
137 Y. Kim, J. W. Hong, Y. W. Lee, M. Kim, D. Kim, W. S. Yun and S. W. Han, *Angew. Chem., Int. Ed.*, 2010, **49**, 10197–10201.
138 M. Bernechea, S. García-Rodríguez, P. Terreros, E. de Jesús, J. L. G. Fierro and S. Rojas, *J. Phys. Chem. C*, 2011, **115**, 1287–1294.
139 S. Alayoglu, A. U. Nilekar, M. Mavrikakis and B. Eichhorn, *Nat. Mater.*, 2008, **7**, 333–338.
140 S. Alayoglu and B. Eichhorn, *J. Am. Chem. Soc.*, 2008, **130**, 17479–17486.
141 A. U. Nilekar, S. Alayoglu, B. Eichhorn and M. Mavrikakis, *J. Am. Chem. Soc.*, 2010, **132**, 7418–7428.
142 B. Lim, M. Jiang, P. H. C. Camargo, E. C. Cho, J. Tao, X. Lu, Y. Zhu and Y. Xia, *Science*, 2009, **324**, 1302–1305.
143 B. Lim, M. Jiang, T. Yu, P. H. C. Camargo and Y. Xia, *Nano Res.*, 2010, **3**, 69–80.

 This journal is © The Royal Society of Chemistry 2011

View Article Online

144 S. Zhou, B. Varughese, B. Eichhorn, G. Jackson and K. McIlwrath, *Angew. Chem., Int. Ed.*, 2005, **44**, 4539–4543.
145 V. M. Dhavale, S. M. Unni, H. N. Kagalwala, V. K. Pillai and S. Kurungot, *Chem. Commun.*, 2011, **47**, 3951–3953.
146 Y. Chen, F. Yang, Y. Dai, W. Wang and S. Chen, *J. Phys. Chem. C*, 2008, **112**, 1645–1649.
147 W. Li and P. Haldara, *Electrochem. Solid-State Lett.*, 2010, **13**, B47–B49.
148 X. Yang, F. Cheng, J. Liang, Z. Tao and J. Chen, *Int. J. Hydrogen Energy*, 2011, **36**, 1984–1990.
149 X. Yang, F. Cheng, Z. Tao and J. Chen, *J. Power Sources*, 2011, **196**, 2785–2789.
150 X.-B. Zhang, J.-M. Yan, S. Han, H. Shioyama and Q. Xu, *J. Am. Chem. Soc.*, 2009, **131**, 2778–2779.
151 G. Chen, S. Desinan, R. Nechache, R. Rosei, F. Roseiacd and D. Ma, *Chem. Commun.*, 2011, **47**, 6308.
152 H. Guo, Y. Chen, X. Chen, R. Wen, G.-H. Yue and D.-L. Peng, *Nanotechnology*, 2011, **22**, 195604.
153 Y. Lu, J. Yuan, F. Polzer, M. Drechsler and J. Preussner, *ACS Nano*, 2010, **4**, 7078–7086.
154 J. Luo, N. Kariuki, L. Han, L. Wang, C.-J. Zhong and T. He, *Electrochim. Acta*, 2006, **51**, 4821–4827.
155 J. Luo, L. Wang, D. Mott, P. N. Njoki, N. Kariuki, C.-J. Zhong and T. He, *J. Mater. Chem.*, 2006, **16**, 1665–1673.
156 C.-J. Zhong, J. Luo, P. N. Njoki, D. Mott, B. Wanjala, R. Loukrakpam, S. Lim, L. Wang, B. Fang and Z. Xu, *Energy Environ. Sci.*, 2008, **1**, 454–466.
157 V. Mazumder, M. Chi, K. L. More and S. Sun, *J. Am. Chem. Soc.*, 2010, **132**, 7848–7849.
158 C. Wang, D. van der Vliet, K. L. More, N. J. Zaluzec, S. Peng, S. Sun, H. Daimon, G. Wang, J. Greeley, J. Pearson, A. P. Paulikas, G. Karapetrov, D. Strmcnik, N. M. Markovic and V. R. Stamenkovic, *Nano Lett.*, 2011, **11**, 919–926.
159 P.-P. Fang, S. Duan, X.-D. Lin, J. R. Anema, J.-F. Li, O. Buriez, Y. Ding, F.-R. Fan, D.-Y. Wu, B. Ren, Z. L. Wang, C. Amatore and Z.-Q. Tian, *Chem. Sci.*, 2011, **2**, 531–539.
160 H. Wang, R. Wang, H. Li, Q. Wang, J. Kang and Z. Lei, *Int. J. Hydrogen Energy*, 2011, **36**, 839–848.
161 J. Zhao, K. Jarvis, P. Ferreira and A. Manthiram, *J. Power Sources*, 2011, **196**, 4515–4523.
162 A. B. Hungria, R. Raja, R. D. Adams, B. Captain, J. M. Thomas, P. A. Midgley, V. Golovko and B. F. G. Johnson, *Angew. Chem., Int. Ed.*, 2006, **45**, 4782–4785.
163 A. Tompos, J. L. Margitfalvi, M. Hegedűs, Á. Szegedi, J. L. G. Fierro and S. Rojas, *Comb. Chem. High Throughput Screening*, 2007, **10**, 71–82.
164 N. Toshima, R. Ito, T. Matsushita and Y. Shiraishi, *Catal. Today*, 2007, **122**, 239–244.
165 T. Matsushita, Y. Shiraishi, S. Horiuchi and N. Toshima, *Bull. Chem. Soc. Jpn.*, 2007, **80**, 1217–1225.
166 P. Venkatesan and J. Santhanalakshmi, *Langmuir*, 2010, **26**, 12225–12229.
167 P. Venkatesan and J. Santhanalakshmi, *J. Mol. Catal. A: Chem.*, 2010, **326**, 99–106.
168 Y. Zhou, S. Wang, B. Ding and Z. Yang, *J. Sol-Gel Sci. Technol.*, 2008, **47**, 182–186.
169 G. Wu, K. L. More, C. M. Johnston and P. Zelenay, *Science*, 2011, **332**, 443–447.

Downloaded by University of Science and Technology of China on 06/05/2013 14:52:51.
Published on 08 August 2011 on http://pubs.rsc.org | doi:10.1039/C1JM12020D